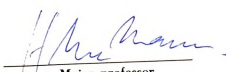THE OPTICAL POTENTIAL IN PROTON - NUCLEUS
SCATTERING

Thesis for the Degree of Ph. D.
MICHIGAN STATE UNIVERSITY
DONALD A. SLANINA
1969

This is to certify that the

thesis entitled

THE OPTICAL POTENTIAL IN

PROTON-NUCLEUS SCATTERING

presented by

Donald A. Slanina

has been accepted towards fulfillment
of the requirements for

Ph.D. degree in Physics

_____
Major professor

Date May 14, 1969

O-169

ABSTRACT

THE OPTICAL POTENTIAL IN PROTON-NUCLEUS SCATTERING

By

Donald A. Slanina

The optical potential for 40 MeV protons is calculated for the spin zero nuclei $^{12}$C, $^{40}$Ca, $^{58}$Ni, $^{120}$Sn, and $^{208}$Pb. The real central part of the potential is calculated to first order in the nucleon-nucleon effective interaction which is taken to be the G-matrix used in studies of the bound state properties of finite nuclei. The impulse approximation is used for an estimate of the spin orbit potential. The imaginary part of the optical potential is calculated from a perturbation treatment of the channels open for inelastic scattering. The energy dependence, isobaric dependence, effect of possible proton-neutron density differences, and antisymmetrization effects are considered for the real part of the central potential. Cross sections are calculated for the scattering of 20 and 40 MeV protons on $^{12}$C and $^{40}$Ca using the theoretical optical potential and compared to cross sections obtained from empirical optical potentials.

THE OPTICAL POTENTIAL IN PROTON-NUCLEUS SCATTERING

By

Donald A. Slanina

A THESIS

Submitted to

Michigan State University

in partial fulfillment of the requirements

for the degree of

DOCTOR OF PHILOSOPHY

Department of Physics and Astronomy

1969

TABLE OF CONTENTS

# LIST OF TABLES

# I. INTRODUCTION

The optical potential is calculated for 40 MeV protons and the spin zero nuclei $^{12}$C, $^{40}$Ca, $^{58}$Ni, $^{120}$Sn, and $^{208}$Pb. To first order in the nucleon-nucleon effective interaction, t(r), the optical potential V(r) is written as a folded integral of t(r) and the nucleon point density or matter density $\rho_m(r)$[1]

$$V(r) = A \int t(|\underline{r}' - \underline{r}|) \rho_m(\underline{r}') d\underline{r}' \tag{1}$$

The effective interaction t(r) must be a continuation of the effective interaction G(r)[2], derived from free nucleon-nucleon scattering data and used in calculating the bound state properties of nuclei. Such an interaction is state dependent and is different in different relative angular momentum states. To calculate the folded integral easily, it is necessary to have the effective interaction expressed in configuration space and the only angular momentum projection for which this is easy to accomplish is the separation of the interaction into parts acting in even and odd relative states. However, the interaction is strongest in s-states and, for hard core potentials like the Hamada-Johnston[3], can be approximated in this and other even states using a Scott-Moszkowski[4] separation distance method giving a configuration space interaction that

vanishes inside the separation distance. In this approximation there is an effective central force in triplet even states arising from the tensor part of nucleon-nucleon force. Thus, the strong part of the force is given mainly as an effective central interaction in configuration space. Estimates for the interaction were taken from Kuo and Brown (KB)[5], Kallio and Kolltveit (KK)[6], and a density dependent interaction designed to mock up the state dependence of the G-matrix from Green[7]. Two forms of Green's density dependent interaction are used; WG having a weaker density dependence than SG. As the last three interactions act only in relative s-states, the further approximation that they are the same in all relative even states is made. Furthermore, since the interaction in relative odd states has little effect on the binding energy of nuclei[8], and is not normally given in configuration space, it is neglected here and $t(r)$ will be set to zero in odd states except for the two-nucleon spin orbit potential. Here the impulse approximation was used to estimate the effective interaction. Motivation for this arises from the successful spin orbit splitting calculations of Elliott et al[9] where the interaction was expressed in terms of free nucleon-nucleon phase shifts. With these approximations, the effective interaction is a central force acting only in relative even states, similar to Serber force, with a separation distance of approximately 1 f, together with a tensor force, negelcted here, and a two body spin-orbit force.

The importance of using a G-matrix effective inter-
action is illustrated by the calculation of the real central
optical potential for $^{40}$Ca and 40 MeV protons using a
Serber type interaction which acts only in relative even
states and fits low energy scattering lengths and effective
ranges[10]. This interaction gave a much larger strength
and range for the optical potential than is empirically
observed or calculated using the G-matrix.

The matter density, assuming no proton-neutron
density difference, was obtained by unfolding the finite
electro-magnetic size of the proton from the empirical
charge density. The charge densities of Acker et al[11]
were used for $^{40}$Ca, $^{120}$Sn, and $^{208}$Pb while Hofstader's[12]
values were used for $^{12}$C and $^{58}$Ni. The matter and charge
densities are related by

$$\rho_{ch}(r) = \int \rho_p(|\underline{r}'-\underline{r}|)\rho_m(\underline{r}')d\underline{r}' \tag{2}$$

where ch, p, and m refer to charge, proton, and matter.
The matter density is assumed to have the same algebraic
form as the charge density. The matter parameters were
obtained by matching the empirical charge densities second
and fourth radial moments to those calculated using equation 2.

The calculated optical potentials were compared to
the empirical potentials of Fricke et al[13] for 40 MeV protons
and Greenlees and Pyle[14] for $^{16}$O, rescaling the numbers to
$^{12}$C. With no antisymmetrization and no proton-neutron
density difference, the real central potentials closely
resembled those obtained by empirical analysis. The major
difference occured in the energy dependence.

This difference was accounted for by including antisymmetrization in the scattering process. Antisymmetrization accounted for 80% of the energy variation given in Fricke et al[13]. The potential due to antisymmetrization is non-local and its' local equivalent was estimated using the method of Perey and Saxon[16].

In order to correlate some of the optical model parameters in the empirical analysis, Greenlees et al[14] define a nucleon point density which is independent of the proton density. They then assume a two nucleon interaction with strength and range as parameters, and search on these parameters for best fit. This analysis leads to a large neutron skin, ie. a large difference in $(<r^2>_p - <r^2>_n)^{1/2}$. If this large proton-neutron density difference is used in Equation 1 with a realistic G-matrix effective interaction, the strength and range of the resultant real central potentials overestimate the empirical potentials. Thus, much of the effect attributed to proton-neutron density difference by Greenlees is included in the present G-matrix effective interaction. In contrast to Greenlees, the isobaric analogue state calculations of Nolen et al[17] given a small proton-neutron density difference. On the theoretical side, the Hartree Fock wave functions of Tarbutton and Davies[18] give a small neutron skin. Their values of the mean squared radii, renormalized so that the calculated and empirical proton mean squared radii were equal, were used to estimate the neutron skin for $^{40}$Ca and

$^{208}$Pb. The difference between neutron and proton distribution radius obtained this way for $^{208}$Pb was about half the value obtained by Greenlees and was almost duplicated by a harmonic oscillator shell model calculation. For this, the oscillator constant, taken to be the same for protons and neutrons, was fixed by the mean squared radius of the empirical proton point distribution. The inclusion of this small neutron skin for the four nuclei brought the calculated strength and range of the real central potentials closer to the observed values.

Since the effective interaction used is hermitian the leading term for the imaginary part of the optical potential comes from that part of the second order term in the effective interaction which involves inelastic scattering on the energy shell. It was assumed that, in the sum over intermediate states, only the low lying collective states excited by inelastic scattering are important. The method of Perey and Saxon[16] was again used to estimate the equivalent local potential from the resulting non-local and angular dependent potential. The examples considered are for 20 and 40 MeV protons on $^{12}$C and $^{40}$Ca. The cross sections obtained by using the theoretical optical potential, using the weak Green effective interaction (WG) to estimate the real central part, were calculated and compared to the cross sections obtained by using the empirical optical potentials. The comparison was relatively good in the sense that the general shape of the cross sections are the same.

Chapter II contains a general derivation of the optical potential series and the algebra associated with the antisymmetric part and imaginary part of the potential. The effective interactions used are presented in Chapter III and the nucleon point density is given in Chapter IV. The results are discussed in Chapter V.

## II. GENERAL THEORY

### 1. Optical Potential Series:

The optical potential reduces the nuclear many body scattering problem to the equivalent problem of one particle scattering in a complex potential well. The nuclear T-matrix is reordered so that the variables of the target nucleus are assimilated in an effective potential, the optical potential. The assumptions used in this section are that the nucleon-nucleus potential may be written as a sum of nucleon-nucleon interactions and that antisymmetrization of the incident nucleon with the target nucleons may be neglected. This point will be returned to later.

The Hamiltonian for the system is[1]

$$H = H_n + K + V = H_0 + V \tag{1}$$

where $H_n$ is the nuclear Hamiltonian, $K$ is the kinetic energy of the incident nucleon, and $V$ is the nucleon-nucleus interaction

$$V(r) = \sum_i (|r - z_i|)$$

and

$$H_n U_m(z_1, \ldots, z_A) = E_m U_m(z_1, \ldots, z_A) \tag{2}$$

where $Z_i$ contains the spacial, spin, and isospin coordinates of the $i^{th}$ nucleon in the nucleus.

The nuclear T-matrix is

$$T = V+VGT \tag{3}$$

where $G=(E-H_0+i\varepsilon)^{-1}$. For elastic ground state scattering we wish to obtain an integral equation for T of the form

$$T_{el} = W+W\bar{G}T_{el} \tag{4}$$

where $\bar{G}$ contains no excited states of the nucleus, W is the optical potential and $T_{el}$ is diagonal with respect to the nuclear ground state. Let n=0 be the nuclear ground state and define the projection operators

$$P = |0><0| \quad ; \quad Q =\sum_{n \neq 0}|n><n|$$

with

$$P+Q=1$$

and

$$T_{el}=PT$$

If we operate with P and Q on Equation 3, we obtain

$$PT=PV+PVG(P+Q)T$$
$$QT=QV+QVG(P+Q)T \tag{5}$$

or

$$PT=[PV+PVG(1-QVG)^{-1}QV][1+GPT]$$

and the optical potential is

$$W= PV+PVG(1-QVG)^{-1}QV \tag{6}$$

to first order: $W \simeq U^1 = PV$

to second order: $W \simeq U^1 + U^2 = PV + PVGQV$

If $U^1$ is written in coordinate representation,

$$U^1(r) = A \int t(|\underline{r}' - \underline{r}|) \rho(r') d\underline{r}' \qquad (7)$$

where A is the number of nucleons in the nucleus, t(r) is the effective nucleon-nucleon interaction, assumed to be local, and $\rho$(r) is the density of point nucleons in the nucleus.


## 2. Antisymmetrization Scattering

Including antisymmetrization in the collision process has been considered in detail by Levin[20], the leading term of which replaces the effective interaction t(r) by an operator $t_{as}$(r) which antisymmetrizes the incident particle with one of the nucleons in the nucleus.

$$t_{as}(r) = t(r)[1 - p_t p_s p_\ell] \qquad (8)$$

or

$$= t_D(r) + t_E(r)$$

where $p_t$, $p_s$, and $p_\ell$ exchange the isospin, spin, and spacial coordinates of the two nucleons involved in the collision and D and E refer to the direct and exchange due to antisymmetrization parts of the amplitude. The effective interactions used to estimate the exchange are the density dependent interactions of Green[7], WG and SG, acting only in relative even states. If SE and TE label the singlet even and triplet even parts of the potential,

$$t_{as}(r) = \bar{t}(r)[1+p_\ell] \tag{9}$$

where

$$\bar{t}(r) = \frac{3}{16}[V_{SE}+V_{TE}] - \frac{N-Z}{16A}[V_{SE}-V_{TE}] \tag{10}$$

and N and Z are the number of neutrons and protons in the target nucleus.

In coordinate representation, the first order potential is

$$<\underline{r}'|U^1|\underline{r}> = A<o,\underline{r}'|t_{as}|\underline{r},o> = U_D + U_E$$

where D and E label the direct and exchange parts of $U^1$. In what follows it will be assumed that $\bar{t}(r)$ is a local potential in coordinate space, ie.

$$<\underline{r}_1'\underline{r}_2'|t|\underline{r}_2\underline{r}_1> = t(|\underline{r}_1-r_2|)\delta(\underline{r}_1'-\underline{r}_1)\delta(\underline{r}_2'-\underline{r}_2) \tag{11}$$

As before, the direct term is

$$U_D(r) = A\int\bar{t}(|\underline{r}'-\underline{r}|)\rho(\underline{r}')d\underline{r}' \tag{12}$$

where $\rho(\underline{r}')$ is the ground state density. The exchange term is

$$U_E(\underline{r}',\underline{r}) = A\int d\underline{r}_1 d\underline{r}_1' [\prod_{i=2}^{A} d\underline{r}_i]\bar{t}(|\underline{r}-\underline{r}_1|)<0|\underline{r}_1'><\underline{r}_1|0>\delta(\underline{r}'-\underline{r}_1)$$
$$\delta(\underline{r}_1'-\underline{r}) \tag{13}$$

$$= A\bar{t}(|\underline{r}-\underline{r}'|)\rho(\underline{r},\underline{r}')$$

and

$$\rho(\underline{r},\underline{r}') = \int<0|\underline{r}><\underline{r}'|0>d\underline{r}_2\ldots d\underline{r}_A$$

The exchange potential is non-local and the equivalent local potential $V_E(r)$ is estimated by using a method similar to that used by Perey and Saxon[16] and is defined from the Schroedinger equation.

$$V_E(r)\psi(\underline{r}) = A\int \overline{t}(|\underline{r}-\underline{r}'|)\rho(\underline{r},\underline{r}')\psi(\underline{r}')d\underline{r}' \tag{14}$$

where $\psi(r)$ corresponds to the distorted wave for elastic scattering by the real direct well and

$$\nabla^2\psi(\underline{r}) = -k_\ell^2\psi(\underline{r})$$

where $k_\ell^2$ is the local wave number in the real direct potential well. {See Appendix A for an outline of the same method based on the integral representation of elastic scattering.}

The method starts by taking the Fourier transform of that part of the function that depends on $\underline{s}=\underline{r}'-\underline{r}$, and then expanding the Fourier transform in a Taylor series about some wave number $k_0$.

$$\overline{t}(s) = (2\pi)^{-3}\int d\underline{p}e^{-i\underline{p}\cdot\underline{s}}\,t(p^2) \tag{15}$$

$$= (2\pi)^{-3}\int d\underline{p}e^{-i\underline{p}\cdot\underline{s}}[t(k_0^2)+(p^2-k_0^2)t'+\ldots]$$

$$= [t(k_0^2)-(\nabla_s^2+k_0^2t'+\ldots]\delta(\underline{s})$$

where $t'=\dfrac{dt}{dp^2}\Big|_{p^2=k_0^2}$. $k_0^2$ is a free parameter and its' value is determined by making $(\nabla_s^2+k_0^2)$ as small as possible.

Keeping only the first two terms in Equation 15

$$V_E(r)\psi(r) = A[\{t(k_0^2)-(\nabla_s^2+k_0^2)t'\}\rho(\underline{r},\underline{r}+\underline{s})\psi(\underline{r}+\underline{s})]_{s=0}$$

Since $\nabla_s^2$ operates on $\rho(r,r')$, the density is estimated by

$$\rho(\underline{r},\underline{r}') = 4\sum_{\ell m}\phi_\ell(r)\phi_\ell(r')Y^*_{\ell m}(\hat{r})Y_{\ell m}(\hat{r}') \tag{16}$$

where the sum over $\ell$ goes over all of the occupied $\ell$ subshells in the nucleus, and $\phi_\ell(r)$ is the radial harmonic oscillator wave function for the $\ell^{th}$ subshell with the oscillator constant being determined by the empirical mean squared radius of the density distribution. The

$$\nabla^2 \rho(\underline{r},\underline{r}')\big|_{s=0} = 4\sum_{\ell m}\phi_\ell(r) Y^*_{\ell m}(\hat{r}) \nabla^2 [\phi_\ell(r') Y_{\ell m}(\hat{r}')]_{s=0}$$

$$= \bar{q}^2 \frac{1}{\pi}\sum_\ell (2\ell+1)\phi_\ell^2(r)$$

Consider the term

$$(\nabla_s^2+k_0^2)\rho(r,r')\psi(r')\big|_{s=0} = (k_0^2-k_\ell^2+\bar{q}^2)\rho(r,r)\psi(r) + [\underline{\nabla}\rho(r,r')\cdot\underline{\nabla}\psi(r')]_{s=0}$$

The gradient $\rho$ gradient $\psi$ part of the above will be neglected. If the $\bar{q}^2$ term and the gradient gradient can be neglected, the above equation corresponds to a local density approximation. Perey and Saruis[20] calculate a term of this type, retaining the gradient gradient part, and obtain a small correction to the local density approximation. Thus, the present calculation should give the effect of exchange on the collision process to within 20% or so. The equivalent local exchange potential is

$$V_E(r) = \frac{A}{\pi}[t(k_0^2)-k_0^2+\bar{q}^2-k_\ell^2)t']\sum_\ell (2\ell+1)\phi_\ell^2(r) \tag{17}$$

and $k_0^2$ is the maximum of zero or $k_\ell^2-\bar{q}^2$.

The most important part of the preceeding development is that $t(p^2)$ be smooth enough to be approximated by the first two terms in the Taylor series expansion.

If this were not the case, higher order terms in $(\nabla_s^2 + k_0^2)$ would have to be retained and the complexity of the problem increases by orders of magnitude.

The IA is used to calculate the spin orbit potential and contains the effects of exchange as noted by Takeda and Watson[21]. Hence, the above procedure will not be used for the spin orbit potential.

## 3. Imaginary Optical Potential

In operator form, the first correction to the optical potential of Equation 7 is

$$U^2 = PVGQV$$

and in coordinate representation is

$$\langle \underline{r}' | U^2 | \underline{r} \rangle = \sum_{n \neq 0} (2\pi)^{-3} \int d\underline{p} \langle \underline{r}' o | V | n\underline{r}'' \rangle d\underline{r}'' G_n(p) e^{i\underline{p} \cdot (\underline{r}'' - \underline{r}''')} d\underline{r}'''$$
$$\times \langle \underline{r}''' n | V | o\underline{r} \rangle \tag{18}$$

where

$$G_n(p) = [\frac{\hbar^2 k^2}{2m} - E_n - \frac{\hbar^2 p^2}{2m} + i\varepsilon]^{-1}$$

n labels the excited states of the nucleus, and the matrix elements of V are related to the form factors used in the calculation of the inelastic scattering amplitudes. Since the interaction depends on spin and isospin, the integration over $\underline{p}$ includes a sum over spin projections. Let V be a local real interaction and let a', b, and a refer to the spin-isospin state of the incident proton. Then

$$\langle \underline{r}' | U^2 | \underline{r} \rangle = \sum_{n \neq 0} (2\pi)^{-3} \frac{1}{2} \sum_{m_a' m_b m_a} \int d\underline{p} \langle a'o | V | nb \rangle G_n(p)$$
$$\times e^{i\underline{p} \cdot (\underline{r}' - \underline{r})} \langle bn | V | oa \rangle \tag{19}$$

The 1/2 arises from the average over final spin projections.

Equation 19 will be used to estimate the imaginary part of the optical potential. Since V is real, the imaginary term comes from the on energy shell part of $G_n(p)$; ie. those inelastic states which can be energetically excited. The calculational model neglects all other intermediate states such as pick up. The real part of the second order term corresponds to the term used to estimate the effects of core correlations on the binding energy and its' effect is small[8]. The imaginary potential is then

$$W(\underline{r}';\underline{r}) = -\frac{\pi}{2(2\pi)^3} \sum_{n \neq 0} \sum_{m_a' m_b m_a} \int d\underline{p} e^{i\underline{p} \cdot (\underline{r}' - \underline{r})} \delta\left(\frac{\hbar^2 k^2}{2m} - E_n - \frac{\hbar^2 p^2}{2m}\right) \tag{20}$$
$$\times \langle a'o | V | nb \rangle \langle bn | V | oa \rangle$$

If $k_n^2 = k^2 - \frac{2mE_n}{\hbar^2}$, then

$$\delta\left(\frac{\hbar^2 k_n^2}{2m} - \frac{\hbar^2 p^2}{2m}\right) = \frac{m}{\hbar^2 p} \delta(p - k_n)$$

Let $\underline{s} = \underline{r}' - \underline{r}$ and integrate equation 20 over p. The result is

$$W(\underline{r}', \underline{r}) = -\frac{m}{4\pi\hbar^2} \sum_{n \neq 0} \sum_{m_a' m_b m_a m_n} \frac{\sin(k_n s)}{s} \sum_{\substack{LSm \\ L'S'm'}} \tilde{F}^{LSJn \ Tn}(r) \tilde{F}^{L'S'Jn \ Tn}(r')$$

$$\times Y_{LM}^*(\hat{r}) Y_{L'M'}(\hat{r}') \langle \tfrac{1}{2} \tfrac{1}{2} m_a -m_b | S m_a -m_b \rangle \langle \tfrac{1}{2} \tfrac{1}{2} m_{a'} -m_b | S' m_{a'} -m_b \rangle$$

$$\times \langle LS M m_a -m_b | J_n M_n \rangle \langle L'S' M' m_{a'} -m_b | J_n M_n \rangle \tag{21}$$

where the F's are the form factors for the inelastic scattering from the ground state to an excited state n and are defined in Appendix B. Thus, the imaginary potential is both non-local and angular dependent.

The major contribution to Equation 21 arises when the spin transferred is zero, $S=S'=0$. This removes the Clebsch-Gordon coefficients from Equation 21 and

$$W(r,r') = -\frac{m}{4\pi\hbar^2} \sum_{J}' \frac{\sin(k_n s)}{s} F^J(r)F^J(r') \sum_{M} Y_{JM}^*(\hat{r})Y_{JM}(\hat{r}')$$

where the prime indicates that the contribution of the ground state is to be omitted and $F^J(r) = \tilde{F}^{JOJ,T}(r)$

The procedure of obtaining the equivalent local potential is more complicated than it was for the exchange potential: $\sin(k_n s)/s$ does not have a useful Fourier transform which can be expanded in a Taylor series. To obtain a suitable Fourier transform, a function of s, $f(s)$, should be taken out of $F^J(r)F^J(r')$ such that $f(s) \sin(k_n s)/s$ does have a Fourier transform. The same effect should be produced by multiplying Equation 22 by

$$1 = e^{-as^2} e^{+as^2}$$

and let

$$g(s) = e^{-as^2} \sin(k_n s)/s$$

$$G^J(r,s) = e^{as^2} F^J(r') \tag{23}$$

Here a is a free parameter and its' value is determined from the condition that

$$g(q^2) \approx g(k_0^2) + (q^2 - k_0^2) \frac{d}{dq^2} g(q^2) \Big|_{q^2 = k_0^2} \qquad (24)$$

over the interesting range of $q^2$ where $g(q^2)$ is the Fourier transform of $g(s)$. The value of a used is $a=1.0$ as it gave a $g(q^2)$ that was approximately linear.

The local equivalent potential was then found by using the Perey-Saxon[16] method previously outlined. Here $k_0^2$ will be the lab energy wave number and $\Psi(\underline{r})$ will correspond to the distorted wave corresponding to elastic scattering by the real potential well.

$$k_0^2 = \frac{2m}{\hbar^2} E_{lab}$$

The equations needed for the potential are

$$\nabla^2 \psi(r) = -k_\ell^2 \psi(r)$$

$$k_\ell^2 = \frac{2m}{\hbar^2} [E_{lab} - V_{REAL}(r)]$$

$$\nabla^2 [G^J(r,s) Y_{LM}(\hat{r}')]_{s=0} = [6aF^J(r) + \hat{F}^J(r)] Y_{LM}(\hat{r})$$

where

$$\hat{F}^J(r) = [\frac{1}{r^2} \frac{d}{dr} r^2 \frac{d}{dr} F^J(r) - \frac{J(J+1)}{r^2} F^J(r)]$$

and

$$\frac{2J+1}{4\pi} = \sum_M Y_{JM}^*(\hat{r}) Y_{JM}(\hat{r})$$

Also the gradient gradient term will again be neglected, giving a local equivalent imaginary optical potential of

$$W_L(r) = -\frac{m}{16\pi^2 \hbar^2} \sum_J{}' (2J+1) X^J(r) F^J(r) \qquad (25)$$

where

$$X^J(r) = [g(k^2) - 6a\frac{d}{dq^2}\,g(q^2)\big|_{q^2=k_0^2}]F^J(r) - \hat{F}^J(r) \qquad (26)$$

The question of convergence is more important here than it was for the exchange potential mainly because the imaginary poential is not a small effect added to a much larger potential. In general, convergence will be served if Equation 25 is relatively insensitive to changes in $k_0^2$. For small values of r, the above holds but inelastic studies[22] indicate that convergence may be a more serious problem at the nuclear surface.

To calculate the contribution from the on energy shell inelastic scattering states it was assumed that the most important contributing inelastic scattering states are the low lying collective states which include the effects of long range correlations. The effect of long range correlations on the imaginary potential wa studied by Terasawa[23] and he found that pairing correlations enhanced the potential by a factor of three. Thus, the strongly correlated states should be the most important and these are the strongly excited T=0 states, $2^+$ and $3^-$ in $^{12}C$ and the $3^-$ and $5^-$ in $^{40}Ca$. An energy weighted sum rule was used to estimate the strengths of the higher excited states of a given multipole.

The low lying collective state wave functions for $^{12}C$ and $^{40}Ca$ were taken from Gillet and Sanderson.[24] The $0^+$, $2^+$, and $4^+$ states are important in $^{40}Ca$ but were not available in Reference 24. These states were then assumed to be a sum of all energetically possible $2\hbar\omega$ particle-hole pairs. This procedure will underestimate their contribution to the imaginary potential because of the importance of correlations[23].

A sum rule is used to estimate the strengths of the higher lying collective states of a given multipole. The energy weighted sum rule is taken from Lane[25] and is a measure of the total electromagnetic transition strength of a given multipole J,

$$S^J = \sum_n (E_n - E_0) \, |<n| \, <\sum_i r_i{}^J Y_{Jo}(\hat{r}_i) \, |o>|^2 \qquad (27)$$

and

$$S^J = \frac{\hbar^2 A}{8\pi m} J(2J+1) \int r^J \rho(r) \, d\underline{r} / \int \rho(r) \, d\underline{r} \qquad (28)$$

where $E_n$ is the energy of the $n^{th}$ excited state of multipole J and $\rho(r)$ is the nucleon density of the nucleus. Now, the inelastic scattering matrix elements are very similar to those in Equation 27 and it will be assumed that Equation 27 is a good estimation of the relative strengths of the inelastic scattering states corresponding to a multipole J.

Consider Equation 27 to be rewritten as

$$S^J = S^J_1 + \bar{S}^J_2$$

where $S_1^J$ is the transition strength of the low lying

state, n=1 in Equation 27, and $\bar{S}_2^J$ will contain the rest of

the transition strength of the multipole J.  Then $\bar{S}_2^J$

will be considered as a pseudo-state which lies $1\hbar\omega$

higher in energy than the lowest collective state.  The

value of $\bar{S}_2^J$ is obtained using Equations 28 and 29 where

$S_1^J$ is calculated using the wave functions in Reference 27.

The wave function associated with $\bar{S}_2^J$ is then considered

to be of the same form as the low lying state but rescaled

by a value associated with $\bar{S}_2^J$.

## III. EFFECTIVE INTERACTIONS

### 1. Impulse Approximation

The impulse approximation effective interaction
(IA) comes from solving the free nucleon-nucleon t-matrix.
It is basically a high energy approximation as it neglects
the binding of the struck nucleon. Watson and Takeda[21]
place the lower limit of its' application at around 100 MeV.

The impulse approximation presented here will
include off energy shell kinematics. The nucleon-nucleon
collision will conserve energy in the nucleon-nucleus
center of mass system but not in the nucleon-nucleon
center of mass system. The ansatz used will be that the
momentum transferred, q, is the same in both systems.
This is equivalent to taking nuclear recoil into account.
Under this ansatz, the final nucleon-nucleon center of
mass momentum is

$$k'^2 = k^2 + \frac{A-1}{A} q^2 \qquad (1)$$

where A is the number of nucleons in the target and k is
the initial nucleon-nucleon center of mass momentum.

For elastic scattering from spin zero nuclei, the
relevant part of the nucleon-nucleon t-matrix is

$$t(q) = A(q) + C(q) \underline{\sigma} \cdot \hat{n} \qquad (2)$$

where $A(q)$ and $C(q)$ are the appropriate Wolfenstein[26] parameters and $\hat{n}$ is a unit vector perpendicular to the scattering plane. These parameters are still operators in isospin space, ie.

$$A(q) = A_0(q) + A_1(q)\, \underline{\tau}_1 \cdot \underline{\tau}_2$$

The calculation uses the Hamada-Johnston potential and the off energy shell matrix elements are calculated by the method Sobel[27] used in his bremsstrahlung calculation. The algebra necessary to obtain the pseudo phase shifts is presented in Appendix C and the expressions for the Wolfenstein parameters in terms of the reaction matrix elements proceeds in the standard manner[26].

The amplitudes $A(q)$ and $C(q)$ are fitted to a sum of two Yukawas and, in order to obtain an idea of their strength and range, they are fitted to a one Yukawa potential in which the range is obtained from the mean squared radius of the two Yukawa fit. Let $t(q)$ stand for either $A(q)$ or $C(q)$, then

$$t(q) = 4\pi \left[ \frac{V_1}{a_1(q^2 + a_1{}^2)} + \frac{V_2}{a_2(q^2 + a_2{}^2)} \right] \qquad (3)$$

or

$$t(r) = V_1 e^{-a_1 r}/a_1 r + V_2 e^{-a_2 r}/a_2 r$$

and

$$t(r) = V_0 e^{-ar}/ar$$

The values of the parameters of the Yukawa potentials that are used are listed in Table 1.

The IA was used to calculate the real central potential, but its' main purpose is to estimate the spin orbit potential for reasons mentioned in the introduction.

## 2. G-Matrix Effective Interactions

At low incident lab energies, the best estimates for the effective interaction should arise from the continuation in energy of the G-matrix interaction used in bound state calculations. Like the impulse approximation t-matrix approach, they are based on low energy free nucleon-nucleon scattering but they also describe nucleon-nucleon scattering in a finite nucleus. As explained in the introduction, they act mainly in relative even states, resembling a Serber force, and will be zero inside a separation distance, d. Under these assumptions, proton-proton (pp) and neutron-proton (np) parts of the inter-action are

$$t_{pp}(r) = \frac{1}{4}V_{SE}(r) \quad ; \quad t_{np}(r) = \frac{1}{8}V_{SE}(r) + \frac{3}{8}V_{TE}(r)$$

where SE and TE refer to the singlet even and triplet even parts of the force.

All of the G-matrix effective interactions are given as effective central interactions. The first estimate comes from Kuo and Brown[5]

$$V_{SE}(r) = v_{c\ell}(r) \qquad\qquad r > d_s \quad : \; = 0 \quad r < d_s$$

KB

$$V_{TE}(r) = v_{c\ell}(r) - 8v_{t\ell}^2(r)/240 \quad r > d_t \quad : \; = 0 \quad r < d_t$$

where $v_{c\ell}$ and $v_{t\ell}$ are the long range parts of the Hamada-Johnston potential for the central and tensor components, respectively. For lab energy of 40 MeV, the separation distances are

$$d_s = 1.05 \; f \qquad ; \qquad d_t = 1.07 \; f$$

The next estimate comes from the studies of Kallio and Kolltveit[6]

$$V_{SE}(r) = -330.8e^{-2.4021(r-.4)} \qquad r > d_s \quad : \; = 0 \quad r < d_s$$

KK

$$V_{TE}(r) = -475.0e^{-2.5214(r-.4)} \qquad r > d_t \quad : \; = 0 \quad r < d_t$$

and, for 40 MeV protons, the separation distances are

$$d_s = 1.046 \qquad ; \qquad d_t = 0.924$$

The effective interaction of Green[7], using the KK interaction, used the local density to account for the state dependence of the interaction.

$$V_{SE}(r) = C_s(1 - a_s\rho^{2/3})v_{SE}^{KK}(r) \qquad r > d_s \quad : \; = 0 \quad r < d_s$$

Green

$$V_{TE}(r) = C_t(1 - a_t\rho^{2/3})v_{TE}^{KK}(r) \qquad r > d_s \quad : \; = 0 \quad r < d_s$$

where WG:

$$C_s = .992 \qquad\qquad a_s = .035$$

$$C_t = 1.071 \qquad\qquad a_t = 1.454$$

SG:

$$C_s = 1.157 \qquad\qquad a_s = .323$$

$$C_t = 1.623 \qquad\qquad a_t = 1.845$$

and $\rho$ is the local density. This interaction uses the KK separation distances.

# IV. NUCLEON DENSITY

The nucleon densities for the target nuclei were obtained from the electron-nucleus scattering results of Hofstader[12] for $^{12}$C and $^{58}$Ni and the muon-nucleus scattering results of Acker et al[11] for $^{40}$Ca, $^{120}$Sn, and $^{208}$Pb. The proton point distribution is obtained by unfolding the finite electromagnetic size of the proton from the empirical charge distribution[28].

$$\rho_{ch}(r) = \int \rho_p(|\underline{r}' - \underline{r}|) \rho_m(\underline{r}') d\underline{r}' \tag{1}$$

where ch, m, and p refer to the charge, proton point, and proton densities. It was assumed that $\rho_{ch}$ and $\rho_m$ were of the same algebraic form. The proton density used was of the form

$$\rho_p(r) = \pi^{-3/2} a_p^{-3} e^{-r^2/a_p^2} \quad ; \quad a_p^2 = 0.427 \tag{2}$$

and the target nuclei were of Woods-Saxon form

$$\rho(r) = \rho_0 [1 + e^{(r-c)/a}]^{-1} \tag{3}$$

Equation 1 gives relations between the radial moments of the three distributions.

$$\langle r^2 \rangle_m = \langle r^2 \rangle_{ch} - \langle r^2 \rangle_p$$

$$\langle r^4 \rangle_m = \langle r^4 \rangle_{ch} - \langle r^4 \rangle_{ch} - \langle r^4 \rangle_p - \frac{10}{3} \langle r^2 \rangle_{ch} \langle r^2 \rangle_p \tag{4}$$

25

These moments are, for a Woods-Saxon distribution,

$$\langle r^2 \rangle = .2c^2(3+7\chi)$$

$$\langle r^4 \rangle = c^4(3+18\chi+31\chi^2)/7$$

$$\chi = (\frac{\pi a}{c})^2$$

The proton point parameters, $c_m$ and $a_m$, were obtained by solving the two equations in Equation 4. Then

$$\chi_m = (\frac{\pi a_m}{c_m})^2$$

$$(49y-31)\chi_m^2 + (42y-18)\chi_m + 9y-3 = 0$$

where

$$y = 7\langle r^4 \rangle_m / 25 \langle r^2 \rangle_m^2$$

and $c_m$ and $a_m$ are obtained from

$$c_m^2 = 5\langle r^2 \rangle_m / (3+7\chi_m)$$

$$a_m^2 = \chi_m c_m^2 / \pi$$

Of the neutron distribution is assumed to be the same as the proton point distribution, the above parameters are those to be used for the matter distribution. Tarbutton and Davies[18] found a small difference between the neutron and proton densities in their Hartree-Fock calculations and their results were closely duplicated for $^{208}$Pb by using the harmonic oscillator shell model picture of the nucleus. The shell model proton density was assumed to be spherical and of the form

$$\rho(r) = \frac{1}{\pi} \sum_{\ell} (2\ell+1) \phi_\ell^2(r)$$

where the sum over $\ell$ goes over all the filled $\ell$ subshells and $\phi_\ell(r)$ is the radial harmonic oscillator wave function for the $\ell^{th}$ subshell. The harmonic oscillator constant, $\alpha$, is obtained from the charge density by using Equation 4 and the neutron density is obtained from this $\alpha$ and using the lowest filled neutron states.

The values used for the density parameters are listed in Table 2. For a further explanation of the symbols used and a discussion concerning the replacement of the pure oscillator wave functions used in Equation 5 by Hartree-Fock wave functions, see Appendix D along with Table 3 and Figure 1.

## V. DISCUSSION

The first part of the optical potential that will be considered is the real central potential. Initially, exchange scattering and a possible proton-neutron density difference will be neglected. Under these assumptions, the potentials obtained are listed in Table 4 and Figures 2 and 3 with

$$U_R = \int V(r) \, d\underline{r} \tag{1}$$

and

$$r^2 = \int r^2 V(r) \, d\underline{r} / U_R \tag{2}$$

The theoretical potentials are compared to the 30 MeV proton analysis of Greenlees et al[14] and the 40 MeV proton analysis of Fricke et al[13].

The agreement of the potentials between themselves and to the empirical potentials is good considering the calculation is a first order one and that rather rough approximations to the G-matrix were made. The major point is that the theoretical potentials which come the closest to matching the empirical potentials are those based on the G-matrix problem for finite nuclei which do take into account, even if only approximately, nucleon-nucleon phase shifts up to several hundred MeV and the

28

presence of other nucleons. The importance of using a
G-matrix based effective interaction was illustrated by
using a Yukawa force, acting only in relative even states,
taken from Preston[10] to calculate the real central potential.
This interaction fits low energy nucleon-nucleon scatter-
ing lengths and effective ranges but using it to calculate
the optical potential gives a much stronger potential
than the empirical potentials. For 40 MeV protons incident
on $Ca^{40}$, the Preston interaction gives a potential with
$U_R$=-22,400 MeV $f^3$ and $<r^2>$=24 $f^2$ while the empirical
potential[13] of F gives $U_R$=-15,330 MeV $f^3$ and $<r^2>$=16.43 $f^2$
and the weak Green (WG) G-matrix interaction gives a
potential with $U_R$=-12,910 MeV $f^3$ and $<r^2>$=15.12 $f^2$.
The same result occurs when the Preston interaction is
used for $^{208}Pb$. The resulting optical potential has
$U_R$=-116,300 MeV $f^3$ and $<r^2>$=41.92 $f^2$ compared to the
empirical values[13] of $U_R$=-79,200 MeV $f^3$ and $<r^2>$=37.19 $f^2$
and the theoretical values, again based on the weak Green
G-matrix interaction, of $U_R$=-69,000 MeV $f^3$ and $<r^2>$=33.80 $f^2$.

Two other characteristics of the real central
potential should also be considered. In the analysis of
Fricke et al[13], the strength of the real central potential
varies with respect to energy and neutron excess as

$$V(r=0)=V_0+V_E E_{LAB}+V_I [\frac{N-Z}{A}] \qquad (3)$$

where $V_0 = 41.1$ MeV, $V_E = -.22$ MeV, $V_I = 26.4$ MeV, and the Coulomb term was suppressed. The theoretical direct potentials gave almost no energy dependence but gave approximately the proper isobaric dependence, see Table 5. The WG and SG potentials are used to consider the effects of exchange and neutron-proton density difference on the characteristics of the real central potential.

The effects of exchange on $U_R$, $<r^2>$, and the general shape of the WG and SG potentials is small as seen in Table 6 and Figure 4. The inclusion of exchange slightly increases the $<r^2>$ and makes the resultant potential more Woods-Saxon in shape as the exchange contribution of exchange is in the energy dependence. Exchange accounts for 80% of the energy variation between the lab energies of 30 to 40 MeV, see Table 5. The theoretical values of $V_E = -.21 \pm .01$ compare favorably to the value obtained by Fricke et al[13]. Visually, the change of the strength of the potential with energy is given in Figure 5 for $^{12}$C and $^{40}$Ca, and the change of shape with energy is given in Figure 6 for $^{40}$Ca. The concave shape of the energy dependence seen on Figure 5 also seems to be indicated by the empirical analysis of Cameron and van Oers[15] for $^{16}$O. There also appears to be a mass effect for the energy dependence, $V_E$ decreasing with A, but this effect may be beyond the resolution of this calculation.

The empirical analysis of Greenlees et al[14] used the proton-neutron density difference to reduce the number of free parameters used in the search procedure for the optical model potential by relating the real central and real spin orbit mean squared radii to a matter distribution. In terms of the mean squared radii for the real potentials,

real central: $\langle r^2 \rangle_R = \langle r^2 \rangle_{2n,c} + \langle r^2 \rangle_m$

real spin orbit: $\langle r^2 \rangle_{so} = \langle r^2 \rangle_{2n,so} + \langle r^2 \rangle_m$

where 2n refers to nucleon-nucleon and m refers to the matter distribution. The analysis used

$$\xi = \langle r^2 \rangle_{2n,c} + \langle r^2 \rangle_{2n,so} = 2.25 \ f^2$$

The value of $\xi$ was obtained from a best fit search and it leads to a large neutron skin. The values of $\xi$ obtained from the G-matrix effective interactions are $\xi = 5 \pm 1 \ f^2$. Thus, the use of a reasonable G-matrix effective interaction absorbs a large amount of the neutron-proton density difference inferred by Greenlees et al[14].

Another source for the estimate of the neutron-proton density difference is from the theoretical Hartree-Fock calculation of Tarbutton and Davies[19] for $^{40}Ca$ and $^{208}Pb$. They obtain a much smaller neutron skin that Greenlees et al[14] and their values are comparable to the values obtained in the isobaric analogue state calculations of Nolen et al[17]. Since the harmonic oscillator method

outlined in Chapter IV gave a neutron skin similar to the one of Tarbutton and Davies for $^{40}$Ca and $^{208}$Pb, it was used to estimate the neutron distributions for $^{58}$Ni and $^{120}$Sn. The mean squared radii for the various neutron distributions are listed in Table 7. The effect of the density difference on the form of the WG potential is illustrated in Figure 4.

The density difference and exchange effects were included in the WG and SG potentials and are presented in Table 6 and Figure 7. The values of $U_R$ and $V_I$ isolate the WG as the best estimate of the effective interaction. Because of this, the WG potential is used for the real part of the theoretical optical potential for the calculation of the cross sections for $^{12}$C and $^{40}$Ca.

The IA was used to estimate the real spin orbit potential because of the reasons presented in the introduction. Since $\rho(r)$ is Woods-Saxon in form and $<r^2>_{2n,so}$ is small, the potentials are fit to a Woods-Saxon form whose parameters are given in Table 8 and is illustrated in Figure 8. The theoretical representation is good in general and especially good for $^{58}$Ni and $^{120}$Sn.

Despite the assumptions used in the calculation of the imaginary central potential, a surface type peaked potential was obtained which agrees in form with the observed empirical forms, see Figure 9. The major difference is that the theoretical potentials peak inside of

the empirical potentials: The same difficulty occurs
in the microscopic form factors used in inelastic scatter-
ing. Even though the convergence of the Perey-Saxon[16]
method used is difficult to estimate, the method should
give the gross structure of the imaginary part of the
optical potential. The important points of the calcula-
tion are that the strongly excited low-lying collective
states are very important and give a large contribution
to the imaginary potential: The total contribution of
a given multipole to the imaginary potential can be
extracted from the use of a sum rule. A case in point
is that the T=0 $2^+$ state in $^{12}C$ accounts for about 80%
of the calculated potential for 20 MeV protons. The
importance of using collective states was noted by
Teresawa[23] in his calculation of the imaginary potential.
He noted that pairing correlations increased this part
of the potential by a factor of 3. A similar effect
was noted for the T=0 $3^-$ state of $^{40}Ca$. The collective
state gave a contribution of 1.15 MeV for 40 MeV protons
while, if the $3^-$ state was replaced by all possible 1h
particle-hole pairs and its' contribution to the imaginary
potential is certainly underestimated.

The total optical potential for $^{40}Ca$ is illustrated
in Figures 7, 8, and 9 and is compared to the empirical
optical potential of Gray et al[29] at 20 MeV and Fricke
et al[13] at 40 MeV and the total optical potential for $^{12}C$

is illustrated in Figure 10 and is compared to the rescaled
$^{16}O$ parameters of Cameron and van Oers[15]. These optical
potentials, both empirical and theoretical, are used to
calculate the differential cross sections for incident
protons of 20 and 40 MeV. The cross sections obtained
are compared in Figures 11 and 12. The general shape
and magnitude of the cross section based on the theoretical
optical potential is much closer to the empirical cross
section at 20 MeV. To see how much of the discrepancy
was due to the imaginary potential, the cross sections
are also plotted for the case where the theoretical
imaginary potential is replaced by the empirical imaginary
potential. This effect is denoted by crosses in Figure 12.
The agreement is amazingly good at 40 MeV and implies
that only the real potentials are well represented by
the theoretical estimates at that energy. At 20 MeV there
is no noticeable improvement resulting from the interchange
of imaginary potentials. This illustrates that the
theoretical estimate of the imaginary term is approxi-
mately as good as the empirical estimate whereas the
neglected inelastic channels may be important at 40 MeV.

Even with all of the assumptions used in the calculation, the theoretical-empirical agreement of the optical potential is good. The major point of this paper then rests on the consistency of the G-matrix effective interaction which is a good estimate for the optical potential effective interaction, is used in the bound state problem of finite nuclei, and has its' foundation in free nucleon-nucleon scattering.

# REFERENCES

1.  A. K. Kerman, H. McManus and R. M. Thaler, Ann. of
    Phys. $\underline{8}$(1959)551;  H. McManus. Les Mecanismes Des
    Reactions Nucleaires, (Grachen/Saint-Nicolas Press,
    1964 page 289).

2.  T. T. S. Kuo, Nucl. Phys. $\underline{A103}$(1967)71.

3.  T. Hamada and I. D. Johnston, Nucl. Phys. $\underline{34}$(1962)382.

4.  S. A. Moszkowski and B. S. Scott, Ann. of Phys. $\underline{11}$(1960)
    65.

5.  T. T. S. Kuo and G. E. Brown, Phys. Lett. $\underline{18}$(1965 54;
    T. T. S. Kuo and G. E. Brown, Nucl. Phys. $\underline{85}$(1966)40.

6.  A. Kallio and K. Kolltveit, Nucl. Phys. $\underline{53}$(1964)87.

7.  A. M. Green, Phys. Lett. $\underline{24B}$(1967)384;  A. Lande and
    J. P. Svenne, Phys. Lett. $\underline{25B}$(1967)91.

8.  G. E. Brown and C. W. Wong, Nucl. Phys. $\underline{A100}$(1967)241.

9.  J. P. Elliott, H. A. Mavromatis and E. A. Sanderson,
    Phys. Lett. $\underline{24B}$(1967)358.

10. M. A. Preston, Physics of the Nucleus (Addison-Wesley
    Publishing Co., 1962, page 27).

## References (continued)

11. H. L. Acker, G. Backenstoss, C. Daum, J. C. Sens and S. A. DeWit, Nucl. Phys. $\underline{87}$(1966)1.

12. R. Hofstader, Ann. Rev. Nucl. Sci. $\underline{7}$(1957)231; H. F. Ehrenberg, R. Hofstader, U. Meyer-Berkhout, D. G. Ravenhall, and S. S. Sobottka, Phys. Rev. $\underline{113}$(1956)666.

13. M. P. Fricke, E. E. Gross, B. J. Morton and A. Zucker, Phys. Rev. $\underline{156}$(1967)1207.

14. G. W. Greenlees, and G. J. Pyle, Phys. Rev. $\underline{149}$(1966) 836; G. W. Greenlees, G. J. Pyle, Y. C. Yang, Phys. Rev. Lett. $\underline{17}$(1966)33.

15. J. M. Cameron and W. T. H. van Oers, University of California Report, UCLA-10P18-10.

16. F. G. J. Perey and D. S. Saxon, Phys. Lett. $\underline{10}$(1964)107.

17. J. A. Nolen, Jr., J. P. Schiffer and N. Williams, Phys. Lett. $\underline{27B}$(1968)1.

18. R. M. Tarbutton and K. T. R. Davies, (to be published).

19. F. S. Levin, Nucl. Phys. $\underline{46}$(1963)275.

20. F. G. Perey and A. M. Saruis, Nucl. Phys. $\underline{70}$(1965)225.

21. Gyo Takeda and K. M. Watson, Phys. Rev. $\underline{97}$(1955)1336.

22. H. McManus and F. Petrovich, (to be published).

23. Tokuo Terasawa, Nucl. Phys. $\underline{39}$(1962)563.

References (continued)

24. Vincent Gillet and E. A. Sanderson, Nucl. Phys. $\underline{54}$ (1964)472.

25. A. M. Lane, Nuclear Theory (W. A. Benjamin Inc., 1964).

26. H. P. Stapp, T. J. Ypsilantis and N. Metropolis, Phys. Rev. $\underline{105}$(1957)302.

27. M. I. Sobel, Phys. Rev. $\underline{138}$(1965)B1517.

28. L. R. B. Elton, Nuclear Sizes (Oxford University Press, 1961).

29. W. S. Gray, R. A. Kenefick and J. J. Kraushoa, Nucl. Phys. $\underline{67}$(1965)542.

30. F. Petrovich, private communication.

31. D. M. Brink and G. R. Satchler, Angular Momentum (Oxford University Press, 1962).

32. R. Muthukrishnan, private communication.

APPENDIX

APPENDIX A


In Chapter 2, the Schroedinger equation was used to obtain an equivalent local potential from the non-local exchange potential. An alternate way to define the equivalent local potential is by the T-matrix. This approach will be useful for inelastic scattering.

With forces acting only in relative even states, the exchange term in the distorted wave born approximation is built up of components of the form:

$$T_{AS} = \sum_{if} C_{if} \int M_{if}(r_1 r_2) d\underline{r}_1 d\underline{r}_2$$

$$M_{if}(\underline{r}_1\underline{r}_2) = \chi^{-*}(\underline{r}_1) \phi_f^*(\underline{r}_2) V(|\underline{r}_1 - \underline{r}_2|) \phi_i(\underline{r}_1) \chi(\underline{r}_2)$$

where the $\chi$'s are the distorted waves discribing elastic scattering in the final and initial channels and $\phi(r)$ is the wave function of the bound nucleon.

Following Perey and Saxon[16], one takes the Fourier transform of that part of the matrix element which is a function of the non-locality, $\underline{r}_1 - \underline{r}_2 = \underline{s}$ and expand the Fourier transform in a Taylor series about the wave number $k_0$

$$V(s) \simeq (2\pi)^{-3} \int e^{i\underline{\lambda} \cdot (\underline{r}_1 - \underline{r}_2)} [V(k_0^2) + (\lambda^2 - k_0^2)\frac{dv}{dk^2}] d\underline{\lambda}$$

$$= [V(k_0^2) - (\nabla_s^2 + k_0^2)\frac{dv}{dk^2}] \delta(\underline{r}_1 - \underline{r}_2)$$

where

$$\frac{dv}{dk^2} = \frac{dV}{d\lambda^2}\Big|_{\lambda^2 = k_0^2}$$

The wave number $k_0^2$ is a free parameter which will be determined such that the first few terms will be important.

If $\underline{r}_1$ and $\underline{s}$ are chosen to be the independent variables,

$$\int M_{if}(\underline{r}_1, \underline{r}_2)d\underline{s} = \chi^{-*}(\underline{r}_1)\phi_f^*(\underline{r}_1)V(k_0^2)\phi_i(\underline{r}_1)\chi(\underline{r}_1)$$

$$-\chi^{-*}(\underline{r}_1)\phi_i(\underline{r}_1)\frac{dv}{dk^2}[(k_0^2+\nabla^2)\phi_f^*(\underline{r}_1)\chi(\underline{r}_1)]$$

and, if the independent variables are $\underline{r}_2$ and $\underline{s}$,

$$\int M_{if}(\underline{r}_1\underline{r}_2)d\underline{s} = \chi^{-*}(\underline{r}_2)\phi_f^*(\underline{r}_2)V(k_0^2)\phi_i(\underline{r}_2)\chi(\underline{r}_2)$$

$$-\chi(\underline{r}_2)\phi_f^*(\underline{r}_2)\frac{dV}{dk^2}[(k_0^2+\nabla^2)\chi^{-*}(\underline{r}_2)\phi_i(\underline{r}_2)]$$

Coming the two results gives

$$M_{if}(\underline{r}) = \int M_{if}(\underline{r}_1, \underline{r}_2)d\underline{s}$$

$$= \chi^{-*}(\underline{r})\phi_f^*(\underline{r})V(k_0^2)\phi_i(\underline{r})\chi(\underline{r})$$

$$-\frac{1}{2}\frac{dv}{dk^2}\{\chi^{-*}(\underline{r})\phi_i(\underline{r})[(k_0^2+\nabla^2)\phi_f^*(\underline{r})\chi(\underline{r})]$$

$$+[(k_0^2+\nabla^2)\chi^{-*}(\underline{r})\phi_i(\underline{r})]\phi_f^*(\underline{r})\chi(\underline{r})\}$$

also,

$$\nabla^2(\phi_f^*\chi) = -(k_f^2+k^2)\phi_f^*\chi+2(\underline{\nabla}\phi_f^*)-(\underline{\nabla}\chi)$$

$$\nabla^2(\chi^{-*}\phi_i) = -(k'^2+k_i^2)\chi^{-*}\phi_i+2(\underline{\nabla}\chi^{-*})\cdot(\underline{\nabla}\phi_i)$$

where

$$\nabla^2 \phi_f^* = -k_f^2 \phi_f^*, \quad \nabla^2 \chi(r) = -k^2 \chi(r), \text{ etc.}$$

Take 1/2 of the cross term appearing in $M_{if}(r)$ and integrate by parts remembering that $dV/dk^2$ is a function of r because $K_0^2$ will depend on the optical potential. Then

$$(\underline{\nabla}\chi^{-*}) \cdot (\nabla \phi_i) \frac{dV}{dk^2} \phi_f^* \chi$$

goes to

$$\chi^{-*}[(\nabla^2 \phi_i)\frac{dV}{dk^2}\phi_f^* \chi + (\nabla \phi_i) \cdot (\nabla\frac{dV}{dk^2})\phi_f^* \chi + (\nabla \phi_i) \cdot (\nabla \phi_f^*)\frac{dV}{dk^2}\chi + \frac{dV}{dk^2}\phi_f^*$$

$$(\nabla \phi_i) \cdot (\nabla\chi)$$

and

$$\chi^{-*}\phi_i \frac{dV}{dk^2}(\nabla\phi_f^*) \cdot (\nabla\chi)$$

goes to

$$[(\nabla\chi^{-*})(\nabla\phi_f^*)\frac{dV}{dk^2}\phi_i + \chi^{-*}\frac{dV}{dk^2}(\nabla\phi_i) \cdot (\nabla\phi_f^*) + \chi^{-*}\phi_i(\nabla\frac{dV}{dk^2}) \cdot (\nabla\phi_f^*)$$

$$+\chi^{-*}\phi_i\frac{dV}{dk^2}(\nabla^2\phi_f^*)]\chi$$

Now, absorb the $\nabla^2\phi_i$ and $\nabla^2\phi_f^*$ into the non cross term of $M_{if}(\underline{r})$ 

(1)

$$M_{if}^0(\underline{r}) = \chi^{-*}(\underline{r})\phi_f^*(\underline{r})[V(k_0^2) - \{k_0^2 - \frac{1}{2}(k'^2 + k^2)\}\frac{dV}{dk^2}]\phi_i(\underline{r})\chi(\underline{r})$$

and

(2)

$$M_{if}^1(\underline{r}) = \frac{1}{2}\chi^{-*}[(\nabla\phi_i)(\nabla\frac{dV}{dk^2})\phi_f + 2(\nabla\phi_i)(\nabla\phi_f^*)\frac{dV}{dk^2} + \phi_i(\nabla\frac{dV}{dk^2}) \cdot (\nabla\phi_f^*)]\chi$$

$$-\frac{1}{2}(\nabla\chi^{-*})\frac{dV}{dk^2}[\phi_i(\nabla\phi_f^*) - (\nabla\phi_i)\phi_f]\chi + \frac{1}{2}\chi^{-*}[(\nabla\phi_i)\phi_f$$

$$-\phi_i(\nabla\phi_f)]\frac{dV}{dk^2}(\nabla\chi)$$

where

$$M_{if}(\underline{r}) = M^0_{if}(\underline{r}) + M^1_{if}(\underline{r})$$

So if terms like $\nabla\chi^*$ and $\nabla\chi$ are neglected,

$$M_{if}(\underline{r}) = \chi^{-*}(\underline{r})\, F(\underline{r})\, \chi(\underline{r}) \tag{3}$$

and

$$k^2_0 = \frac{1}{2}\text{Real}\,[k'^2 + k^2]$$

$$F(\underline{r}) = \phi^*_f(\underline{r})\, V(k^2_0)\, \phi_i(\underline{r}) + \frac{i}{2}\text{Imag}\,[k'^2 + k^2]\frac{dV}{dk^2}\, \phi^*_f(\underline{r})\, \phi_i(\underline{r})$$

$$+ \frac{dV}{dk^2}(\nabla\phi_i)\cdot(\nabla\phi_f) + \frac{1}{2}(\nabla\frac{dV}{dk^2})\cdot[(\nabla\phi^*_f)\,\phi_i(r) + \phi^*_f(r)\,(\nabla\phi_i)] \tag{4}$$

The expression given in Equations 1 and 2 are similar to those obtained by Perey and Sarius.[20] In Equation 2 the $\nabla\chi$ terms contain a nucleon current density which should approximately be zero for elastic scattering. Also, for elastic scattering, $\chi^{-*}(\underline{r})$ becomes a plane wave.

In this appendix the expression for inelastic scattering form factor, which will be used to calculate the imaginary part of the potential, is presented.[30] The process considered is

$$a+A \to b+B$$

with the matrix

$$<bB|V|Aa>$$

The interaction will neglect exchange, tensor and spin orbit forces, and is

$$V(r) = \sum_{i}^{A} v(|\underline{r}-\underline{r}_i|)$$

and if $\underline{s}=\underline{r}-\underline{r}_1$

$$v(s) = v_{00}(s) + v_{10}(s)(\underline{\sigma}\cdot\underline{\sigma}_i) + v_{01}(s)(\underline{T}\cdot\underline{T}_i) + v_{11}(s)(\underline{\sigma}\cdot\underline{\sigma}_i)(\underline{T}\cdot\underline{T}_i)$$

Using tensor notation for spin and i-spin have

$$\sigma^0 = 1 \qquad\qquad T^0 = 1$$

$$\sigma^1 = \underline{\sigma} \qquad\qquad T^1 = \underline{T}$$

and

$$v(s) = \sum_{stxy} (-)^{x+y} v_{st}(s) \sigma_{-x}^s \sigma_x^s(i) T_{-y}^t T_y^t(i)$$

To aid in the separation of nuclear and interaction information, write

$$v_{st}(s) = \int v_{st}(|\underline{r}-\underline{r}'|)\,\delta(\underline{r}'-\underline{r}_i)\,dr'$$

and expanding both integrands in spherical harmonics

$$v_{st}(s) = \sum_{LM} Y^*_{LM}(\hat{r})\, Y_{LM}(\hat{r}_i) \int v_{stL}(r,r')\,\frac{\delta(r'-r_i)}{r'^2}\,r'^2\,dr'$$

In order to treat spin and space equally, introduce the spherical tensor of rank J as

$$T^{LSJ}_{M_J} = \sum_{M'\chi'} \langle LSM'\chi'|JM_J\rangle Y_{LM'}\,\sigma^S_{\chi'}$$

Also if

$$O^{LSJ,M_J}_{Ty}(r,r') = \sum_i T^T_y(i)\, T^{LSJ}_{M_J}\, v_{STL}(r',r)\,\frac{\delta(r'-r_i)}{r'^2}$$

then

$$\langle bB|V|Aa\rangle = \sum_{\substack{LSTJ\\MxyM_J}} (-)^{x+y}\, Y^*_{LM}(\hat{r})\,\langle LSM_x|JM_J\rangle\langle b|\sigma^S_{-x}T^T_{-y}|a\rangle$$

$$\langle B| \int O^{LSJ,M_J}_{Ty}(r,r')\,r'^2\,dr'\,|A\rangle$$

The processes considered are restricted to those where the i-spin projection of the target and the spin, i-spin, and i-spin projection of the incident nucleus does not change. Upon using the Wigner Eckeart theorm, using the phase conventions of Brink and Satchler,[31] the matrix element becomes

$$\langle bB|V|Aa\rangle = \sum_{LSTJM} (-)^{s_a-m_b}\, \langle\tfrac{1}{2}\,\tfrac{1}{2}m_a-m_b|S\ m_a-m_b\rangle$$

$$\langle J_A J M_A M_B - M_A | J\ M_B\rangle\langle LSMm_a-m_b|JM_B-M_A\rangle$$

$$\langle\tfrac{1}{2}TT_a 0|\tfrac{1}{2}T_a\rangle\langle T_A TT_A 0|T_B T_A\rangle\tilde{F}^{LSJ,T}(r)\,Y^*_{LM}(\hat{r})$$

where

$$\tilde{F}^{LSJ,T}(r) = \int v_{STL}(r,r') F^{LSJ,T}(r') r'^2 dr'$$

and

$$F^{LSJ,T}(r') = \sqrt{2}\ \sqrt{(2T+1)} <\alpha_B J_B T_B ||\sum_i T^T(i) T^{LSJ}(i) \frac{\delta(r'-r_i)}{r'^2}$$

$$||\alpha_A J_A T_A>$$

where the quantum numbers used above are defined in

$$|Aa> = |\alpha_A J_A M_A T_A T_A> |s_a m_a t_a T_a>$$

$$|Bb> = |\alpha_B J_B M_B T_B T_A> |s_a m_b t_a T_a>$$

and L, S, T, and J are the orbital angular momentum, spin, i-spin, and total angular momentum tranferred to the nucleus during the reaction.

APPENDIX C

In an ordinary phase shift calculation[26] the M-matrix is defined from the scattered spherical wave

$$\psi^{sc}(r,\theta,\phi) = M(\theta\phi)|\chi_{inc}> \frac{e^{ikr}}{r}$$

where $\psi^{sc}$ is the scattered wave and $|\chi_{inc}>$ is the initial spin state. M is related to the S-matrix and the R-matrix by

$$S = R + 1$$

and

$$M(\theta\phi) = \sum_{\ell\ell'm'} \frac{1}{ik} [\pi(2\ell+1)]^{1/2} Y_{\ell'm'}(\theta\phi) <\ell'm'|R|\ell o> \tag{1}$$

For the spin zero case, the differential equations we have to solve are

$$\frac{d^2}{dr^2} u_\ell(r) + [k^2 - \frac{\ell(\ell+1)}{r^2} - U(r)] u_\ell(r) = 0 \tag{2}$$

$$\frac{d^2}{dr^2} F_\ell(r) + [k'^2 - \frac{\ell(\ell+1)}{r^2}] F_\ell(r) = 0$$

where $u_\ell(r)$ is the actual wave function and $F_\ell(r)$ is the regular bessel function with the boundry conditions

$$F_\ell(r) \xrightarrow[r\to\infty]{} \sin(k'r - \frac{\ell\pi}{2})$$

$$u_\ell(r) \xrightarrow[r\to\infty]{} \sin(kr - \frac{\ell\pi}{2} + \delta_\ell) \tag{3}$$

From Equations 2 and 3, we get

$$\sin\delta_\ell = -\frac{1}{k}\int_0^\infty F_\ell(k'r)U(r)u_\ell(r)dr$$

This defines the one energy shell phase shift. If k'=k, the pseudo phase shift is defined

$$\Delta_\ell = -\frac{1}{k'}\int_0^\infty F_\ell(k'r)U(r)u_\ell(r)dr \qquad (4)$$

with

$$\Delta_\ell = \sin\delta_\ell \qquad \text{if } k'=k$$

and since

$$<\ell|R|\ell> = 2i|\sin\delta_\ell \qquad \text{for } k'=k$$

then

$$<\ell|R|\ell> = 2i\ \Delta_\ell \qquad \text{for } k'\neq k$$

Once the matrix elements of R are represented in terms of the pseudo phase shifts, the procedure to obtain the Wolfenstein parameters is the same as that for the regular phase shift calculation[26]. Equation 4 holds for $\ell=j$ ($j=\underline{\ell}+\underline{s}$) and s=0 or 1. Since the Hamada-Johnston[3] potential has a tensor part, the wave functions for $\ell=j\pm1$ are coupled. Using Blatt-Biedenharn phase shifts, the equations that are to be solved are

$$[\frac{d^2}{dr^2}+k^2-\frac{(j+1)j}{r^2}-\frac{m}{\hbar^2}V_j^-(r)]u_1^-(r)-\frac{m}{\hbar^2}V_j^0(r)u_1^+(r)=0$$

$$[\frac{d^2}{dr^2}+k^2-\frac{(j+1)(j+2)}{r^2}-\frac{m}{\hbar^2}V_j^+(r)]u_2^+(r)-\frac{m}{\hbar^2}V_j^0(r)u_2^-(r)=0$$

$$(5)$$

where

$$V_j^+ = V_C - (j+2)V_{SL} - [2(j-1)/(2j+1)]V_T - (j+2)V_{LL}$$

$$V_j^- = V_C + (j-1)V_{SL} - [2(j-1)/(2j+1)]V_T + (j-1)V_{LL}$$

$$V_j^0 = \{6[j(j+1)]^{1/2}/(2j+1)\}V_T$$

and C, SL, T, LL refer to the central, spin orbit, tensor and quadratic spin orbit parts of the Hamada-Johnston potential.

These u's are then to be solved for numerically. The u's are then expressed in terms of W's

$$W_1^\pm \to \sin(kr - (j\pm1)\frac{\pi}{2} + \delta_-)$$

$$W_2^\pm \to \sin(kr - (j\pm1)\frac{\pi}{2} + \delta_+)$$

where

$$u_1^\pm = (\frac{\sin\varepsilon_j}{\cos\varepsilon_j})e^{i\delta} - W_1^\pm$$

$$u_2^\pm = (-\frac{\cos\varepsilon_j}{\sin\varepsilon_j})e^{i\delta} + W_2^\pm$$

Then, the pseudo-phase shifts are defined as

$$\Delta_{j-1}^- = I_{j-1}^-(W_1^-) + \tan\varepsilon_j |I_{j-1}^0(W_1^+)$$

$$\Delta_{j-1}^+ = I_{j+1}^+(W_1^+) + \cot\varepsilon_j |I_{j+1}^0(W_1^-)$$

(6)

$$\Delta_{j+1}^- = I_{j-1}^-(W_2^-) = \cot\varepsilon_j |I_{j-1}^0(W_2^+)$$

$$\Delta_{j+1}^+ = I_{j+1}^+(W_2^+) - \tan\varepsilon_j |I_{j+1}^0(W_2^-)$$

where

$$I_{\ell}^{\overset{+}{0}}(f) = -\frac{m}{\hbar^2 k'} \int_0^\infty F_\ell(k'r) V_j^{\overset{+}{0}}(r) f(r) dr \tag{7}$$

Equation 6 arises in the same way as Equation 4 did for the $\ell=j$ case. By using the W's in Equation 6, we have for $k' \to k$

$$\Delta_{j-1}^{\pm} \to \sin\delta_{j-1}$$

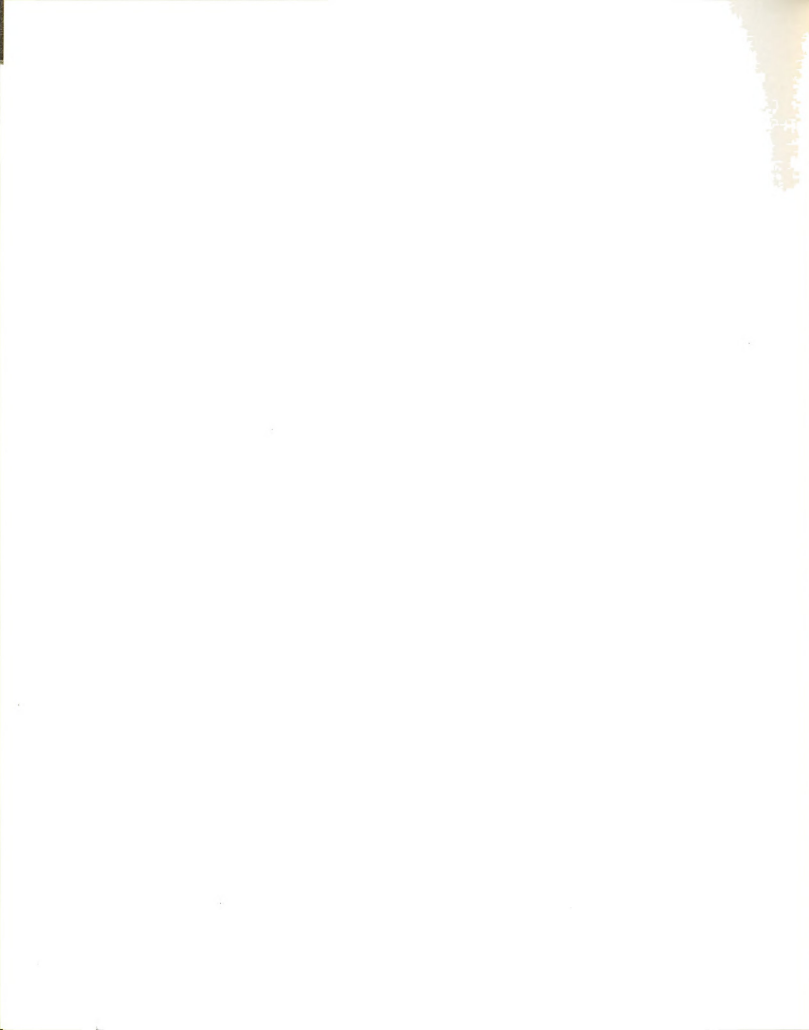$$\Delta_{j+1}^{\pm} \to \sin\delta_{j+1}$$

Then the matrix elements of R become

$$\langle j-1|R|j+1 \rangle = \sin\varepsilon_j \cos\varepsilon_j \left[ e^{i\delta-}\Delta_{j-1}^- - e^{i\delta+}\Delta_{j+1}^- \right]$$

$$\langle j+1|R|j-1 \rangle = \sin\varepsilon_j \cos\varepsilon_j \left[ e^{i\delta-}\Delta_{j-1}^+ - e^{i\delta+}\Delta_{j+1}^+ \right]$$

$$\langle j-1|R|j-1 \rangle = \cos^2\varepsilon_j e^{i\delta-}\Delta_{j-1}^- + \sin^2\varepsilon_j e^{i\delta+}\Delta_{j+1}^-$$

$$\langle j+1|R|j+1 \rangle = \sin^2\varepsilon_j e^{i\delta-}\Delta_{j-1}^+ + \cos^2\varepsilon_j e^{i\delta+}\Delta_{j+1}^+$$

APPENDIX D


The method used to obtain the proton point density, and thus the matter density if there were no neutron skin, from the empirical charge density is outlined in Chapter IV. Table 2 lists the parameters for the nuclei considered where the density is of two forms

$$\text{form 1:} \quad \rho(r) = \rho_0 (1 + c \ r^2/a^2) e^{-r^2/a^2} \tag{1}$$

$$\text{form 2:} \quad \rho(r) = \rho_0 [1 + e^{(r-c)/a}]^{-1} \tag{2}$$


The values of the harmonic oscillator constant $\alpha$ and the energy $\hbar\omega$, where

$$\hbar\omega = \frac{\hbar^2 c^2}{\alpha^2 m_p c^2} \tag{3}$$

and $m_p$ is the proton mass, listed in Table 2 are obtained by matching the oscillator density's mean squared radius to the empirical proton point mean squared radius. In obtaining the oscillator constant, the center of mass correction was included for $^{12}C$ and $^{40}Ca$ but neglected for the rest of the nuclei as it corresponds to a $1/A$ correction.

The example of $^{40}$Ca from Acker et al[11] is used to illustrate the forms of the various distributions and the effect on the oscillator distribution if the pure oscillator radial wave functions are replaced by Hartree-Fock wave functions.

As in Chapter IV, the oscillator density is

$$\rho(r) = \frac{1}{\pi} \sum_{\ell} (2\ell+1) \phi_{\ell}^2(r) \tag{4}$$

but now $\phi_{\ell}(r)$ is replaced by a radial Hartree-Fock wave function

$$\phi_{\ell}(r) = \sum_{m} C_{mn_{\ell}} R_{m\ell}(r)$$

where $R_{m\ell}(r)$ is the radial oscillator wave function for the $\ell^{th}$ subshell (defined by the quantum numbers m and $\ell$). The $^{40}$Ca Hartree-Fock wave functions used[32] are listed in Table 3. Then, in Figure 1, the charge, proton point, proton point oscillator, and the oscillator charges (the distribution obtained by folding the finite electromagnetic size of the proton into the proton point oscillator distribution) densities are given for both pure oscillator and Hartree-Fock wave functions.

TABLE 1

The impulse approximation parameters fit to one and two Yukawas.

| | | $-V_1$ (MeV) | $a_1$ (f$^{-1}$) | $V_2$ (MeV) | $a_2$ (f$^{-1}$) | $<r^2>$ (f$^2$) | $V_0$ (MeV) | $a^*$ (f$^{-1}$) |
|---|---|---|---|---|---|---|---|---|
| $^{40}$Ca | pp | 3480 | 2.44 | 4770 | 2.80 | 3.34 | 55.0 | 1.34 |
| | np | 237 | 1.70 | 418 | 2.62 | 3.19 | 64.6 | 1.37 |
| | so | 952 | 2.90 | 911 | 3.00 | 1.01 | 75.6 | 2.43 |
| $^{58}$Ni | pp | 3400 | 2.44 | 4810 | 2.80 | 3.34 | 54.9 | 1.34 |
| | np | 239 | 1.70 | 428 | 2.62 | 3.22 | 63.8 | 1.36 |
| | so | 1010 | 2.90 | 982 | 3.00 | 1.04 | 71.8 | 2.40 |
| $^{120}$Sn | pp | 2890 | 2.39 | 4140 | 2.80 | 3.39 | 53.7 | 1.33 |
| | np | 143 | 1.70 | 437 | 2.62 | 3.24 | 63.0 | 1.36 |
| | so | 1330 | 2.90 | 1332 | 3.00 | 1.17 | 59.3 | 2.27 |
| $^{208}$Pb | pp | 2450 | 2.39 | 3810 | 2.90 | 3.34 | 55.0 | 1.34 |
| | np | 244 | 1.70 | 439 | 2.62 | 3.25 | 62.7 | 1.36 |
| | so | 1430 | 2.90 | 1450 | 3.00 | 1.21 | 55.8 | 2.23 |

$^*a=[6./<r^2>]^{1/2}$

TABLE 2

The charge and proton point densities.

| | $c_{ch}$ | $a_{ch}$ | $\langle r^2 \rangle_{ch}$ | form | $c_m$ | $a_m$ | $\langle r^2 \rangle_m$ | $\alpha$ (f) | $\hbar\omega$ (MeV) | refer. |
|---|---|---|---|---|---|---|---|---|---|---|
| $^{12}$C | 1.12 | 1.71 | 6.22 | 1 | 1.839 | 1.580 | 5.58 | 1.653 | 15.19 | 12 |
| $^{12}$C | 2.30 | 1.85 | 5.62 | 2 | 2.220 | 1.682 | 4.98 | 1.561 | 17.03 | 28 |
| $^{40}$Ca | 3.64 | 2.50 | 12.41 | 2 | 3.603 | 2.361 | 11.77 | 1.993 | 10.45 | 12 |
| $^{40}$Ca | 3.767 | 2.21 | 12.00 | 2 | 3.746 | 2.029 | 11.36 | 1.958 | 10.82 | 11 |
| $^{58}$Ni | 4.28 | 2.50 | 15.45 | 2 | 4.262 | 2.342 | 14.81 | 2.079 | 9.60 | 12 |
| $^{120}$Sn | 5.48 | 2.21 | 21.50 | 2 | 5.487 | 1.981 | 20.86 | 2.256 | 8.15 | 11 |
| $^{208}$Pb | 6.50 | 2.50 | 29.13 | 2 | 6.511 | 2.068 | 28.49 | 2.438 | 6.98 | 12 |
| $^{208}$Pb | 6.67 | 2.21 | 30.18 | 2 | 6.683 | 1.961 | 29.54 | 2.483 | 6.73 | 11 |

TABLE 3

Hartree-Fock parameters for $^{40}$Ca oscillator constant = a = 2.08f.; energy/nucleon = -7.47 MeV.

| single particle state | single particle state | $C_{0n_\ell}$ | $C_{1n_\ell}$ | $C_{2n_\ell}$ | $C_{3n_\ell}$ |
|---|---|---|---|---|---|
| 1s | -65.0 | .9987 | .0513 | -.0028 | -.0034 |
| 1p | -39.2 | .9989 | .0462 | .0069 | -.0046 |
| 2s | -17.7 | -.0512 | .9971 | -.0423 | .0375 |
| 1d | -18.0 | .9992 | -.0209 | .0316 | -.0109 |

TABLE 4

$U_R$ and $\langle r^2 \rangle$ for only the direct term of the real central potential.

| | $^{40}$Ca $\quad \langle r^2 \rangle_m = 11.36$ | | | | $^{58}$Ni $\quad \langle r^2 \rangle_m = 14.81$ | | |
|---|---|---|---|---|---|---|---|
| type | $-U_R(\mathrm{MeV.f}^3)$ | $\langle r^2 \rangle (f^2)$ | $\langle r^2 \rangle (f^2)_{2B}$ | type | $-U_R(\mathrm{MeV.f}^3)$ | $\langle r^2 \rangle (f^2)$ | $\langle r^2 \rangle (f^2)_{2B}$ |
| IA | 12,031 | 14.52 | 3.16 | IA | 17,470 | 17.98 | 3.15 |
| KB | 14,560 | 18.03 | 6.76 | KB | 21,410 | 21.45 | 6.75 |
| KK | 15,370 | 14.50 | 3.19 | KK | 22,630 | 17.94 | 3.19 |
| WG | 12,910 | 15.12 | 3.76* | WG | 19,020 | 18.75 | 3.94 |
| SG | 15,690 | 15.50 | 4.14* | SG | 23,240 | 19.26 | 4.45 |
| G | 17,160 | 16.78 | | G | 23,690 | 19.72 | |
| F | 15,330 | 16.43 | | F | 21,770 | 19.51 | |

TABLE 4 (continued)

| | 120Sn $\langle r^2 \rangle_m = 20.86$ | | | | 208Pb $\langle r^2 \rangle_m = 29.54$ | | |
|------|-----------------|-----------------|------------------------|------|-----------------|-----------------|------------------------|
| type | $-U_R$(MeV.f$^3$) | $\langle r^2 \rangle$(f$^2$) | $\langle r^2 \rangle$(f$^2$)$_{2B}$ | type | $-U_R$(MeV.f$^3$) | $\langle r^2 \rangle$(f$^2$) | $\langle r^2 \rangle$(f$^2$)$_{2B}$ |
| IA | 36,370 | 24.08 | 3.22 | IA | 63,180 | 32.74 | 3.20 |
| KB | 46,590 | 27.40 | 6.71 | KB | 82,070 | 35.95 | 6.70 |
| KK | 49,550 | 23.97 | 3.17 | KK | 87,480 | 32.64 | 3.17 |
| WG | 39,570 | 24.95 | 4.09 | WG | 68,960 | 33.80 | 4.26 |
| SG | 47,440 | 25.57 | 4.71 | SG | 82,390 | 34.56 | 5.02 |
| G | 50,120 | 27.79 | | G | 88,090 | 37.10 | |
| F | 45,140 | 27.60 | | F | 79,230 | 37.19 | |

F:  Fricke et al [13]

G:  Greenlees et al [14]

$^*\langle r^2 \rangle_{2B}$ for WG and SG defined as

$$\langle r^2 \rangle_{2B} = \langle r^2 \rangle - \langle r^2 \rangle_m$$

and is the effective mean squared radius of the nucleon-nucleon effective interaction.
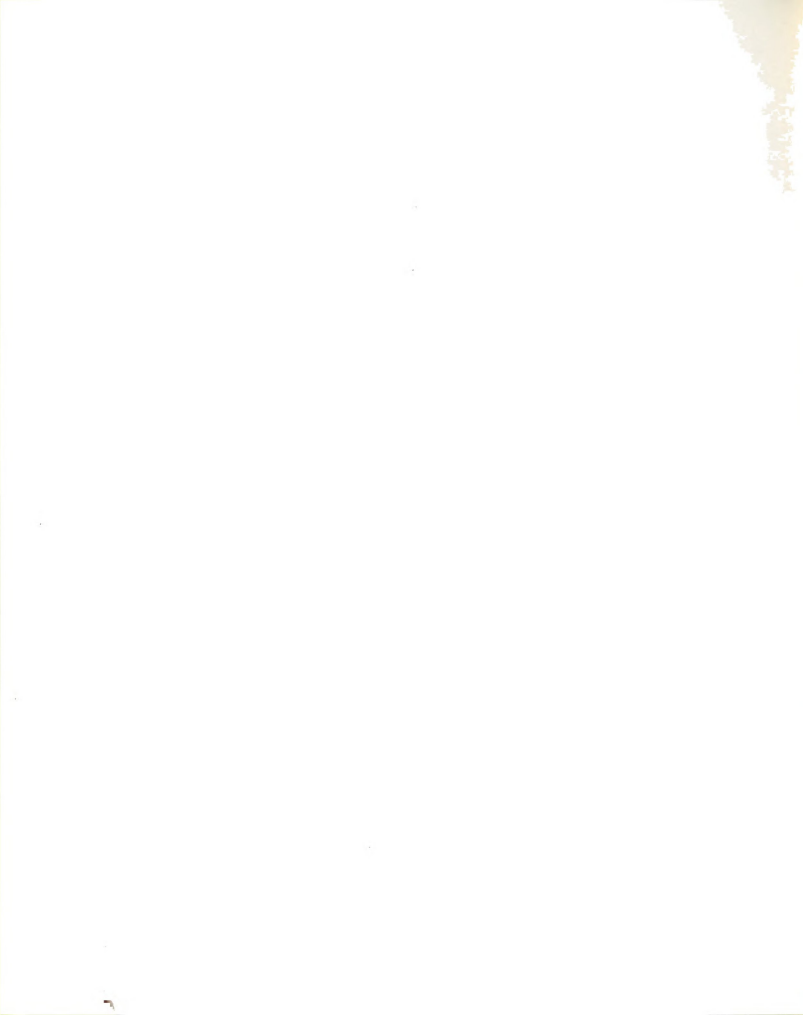
TABLE 5

Energy dependence ($V_E$) and isobaric dependence ($V_I$) of WG and SG for the direct term and the total potential.

| | type | $-V_E(D)$ | $-V_E(T)$ | $V_I(D)$ | $V_I(T)$ |
|---|---|---|---|---|---|
| $^{40}$Ca | WG | .03 | .21 | | |
| | SG | .04 | .20 | | |
| $^{58}$Ni | WG | .03 | .20 | 28.63 | 24.47 |
| | SG | .03 | .20 | 37.12 | 37.76 |
| $^{120}$Sn | WG | .03 | .22 | 28.82 | 26.81 |
| | SG | .03 | .18 | 36.59 | 37.69 |
| $^{208}$Pb | WG | .03 | .22 | 28.76 | 24.68 |
| | SG | .04 | .21 | 36.72 | 36.50 |

where D and T refer to the direct interaction alone and the total interaction.

TABLE 6

$U_R$ and $<r^2>$ for WG and SG for the direct (D), exchange (E), density difference (ρ) and total (T) potentials.

| type | | $-U_R(D)$ | $-U_R(E)$ | $-U_R(\rho)$ | $-U_R(T)$ | $<r^2>_D$ | $<r^2>_E$ | $<r^2>_\rho$ | $<r^2>_T$ |
|---|---|---|---|---|---|---|---|---|---|
| $^{40}$Ca | WG | 12910 | 1730 | 12830 | 14570 | 15.12 | 17.88 | 14.96 | 15.31 |
| | SG | 15690 | 1900 | 15550 | 17450 | 15.50 | 19.37 | 15.35 | 15.79 |
| | F | | | | 15330 | | | | 16.43 |
| $^{58}$Ni | WG | 19020 | 2590 | 19110 | 21700 | 18.75 | 22.69 | 18.95 | 19.40 |
| | SG | 23240 | 2830 | 23420 | 26250 | 19.26 | 24.56 | 19.46 | 20.01 |
| | F | | | | 21770 | | | | 19.51 |
| $^{120}$Sn | WG | 39570 | 4510 | 40190 | 44700 | 24.95 | 35.48 | 25.76 | 26.74 |
| | SG | 47440 | 4830 | 48670 | 53500 | 25.57 | 38.85 | 26.38 | 27.51 |
| | F | | | | 45140 | | | | 27.60 |
| $^{208}$Pb | WG | 68960 | 7820 | 71250 | 79070 | 33.80 | 50.91 | 36.35 | 37.79 |
| | SG | 82390 | 8390 | 86910 | 95300 | 34.56 | 55.84 | 37.10 | 38.75 |
| | F | | | | 79230 | | | | 37.19 |

F: Fricke et al[13]

TABLE 7

$\langle r^2 \rangle$ and Woods-Saxon parameters for proton, neutron and matter distribution.

| | | $\langle r^2 \rangle_p$ | $\langle r^2 \rangle_m$ | $\langle r^2 \rangle_n$ | $c_n$ | $a_n$ | $\langle r^2 \rangle_n^{1/2} - \langle r^2 \rangle_p^{1/2}$ |
|---|---|---|---|---|---|---|---|
| $^{40}$Ca | TD | 11.36 | 11.23 | 11.10 | 3.69 | .461 | -.04 |
| $^{58}$Ni | G | 14.81 | 16.97 | 19.80 | 5.15 | .532 | .60 |
| | HO | 14.81 | 14.97 | 15.12 | 4.32 | .532 | .04 |
| $^{120}$Sn | G | 20.86 | 25.20 | 28.09 | 6.49 | .450 | .73 |
| | HO | 20.86 | 21.54 | 22.03 | 5.66 | .450 | .13 |
| $^{208}$Pb | TD | 29.54 | 31.66 | 33.04 | 7.11 | .446 | .31 |
| | G | 29.54 | 34.11 | 36.97 | 7.55 | .446 | .65 |
| | HO | 29.54 | 32.18 | 33.89 | 7.21 | .446 | .39 |

TD: Tarbutton and Davies[19]          $a_n = a_p$

G: Greenlees et al[14]

HO: Harmonic oscillator basis

TABLE 8

Spin orbit parameters

| | type | $V_0$ (MeV) | $c_{so}$ (f) | $a_{so}$ (f) | $<r^2>_{2n}$ | $U_R$ | $<r^2>$ |
|---|---|---|---|---|---|---|---|
| $^{40}$Ca | IA | 5.17 | 3.68 | .554 | 1.01 | 1320 | 12.37 |
| | G | 5.70 | 3.94 | .70 | | 1920 | 16.08 |
| | F | 6.22 | 3.52 | .778 | | 1680 | 15.78 |
| $^{58}$Ni | IA | 5.04 | 4.19 | .621 | 1.04 | 1890 | 15.85 |
| | G | 5.20 | 3.93 | .70 | | 1735 | 16.03 |
| | F | 5.53 | 4.15 | .641 | | 2040 | 15.99 |
| $^{120}$Sn | IA | 5.19 | 5.42 | .565 | 1.17 | 3833 | 22.03 |
| | G | 6.20 | 5.78 | .700 | | 5743 | 26.82 |
| | F | 6.11 | 5.21 | .800 | | 4470 | 25.15 |
| $^{208}$Pb | IA | 5.05 | 6.63 | .563 | 1.21 | 6600 | 30.75 |
| | G | 5.13 | 6.72 | .700 | | 7230 | 33.90 |
| | F | 5.84 | 6.08 | .794 | | 6421 | 30.88 |

F:  Fricke et al[13]

G:  Greenlees et al[14]
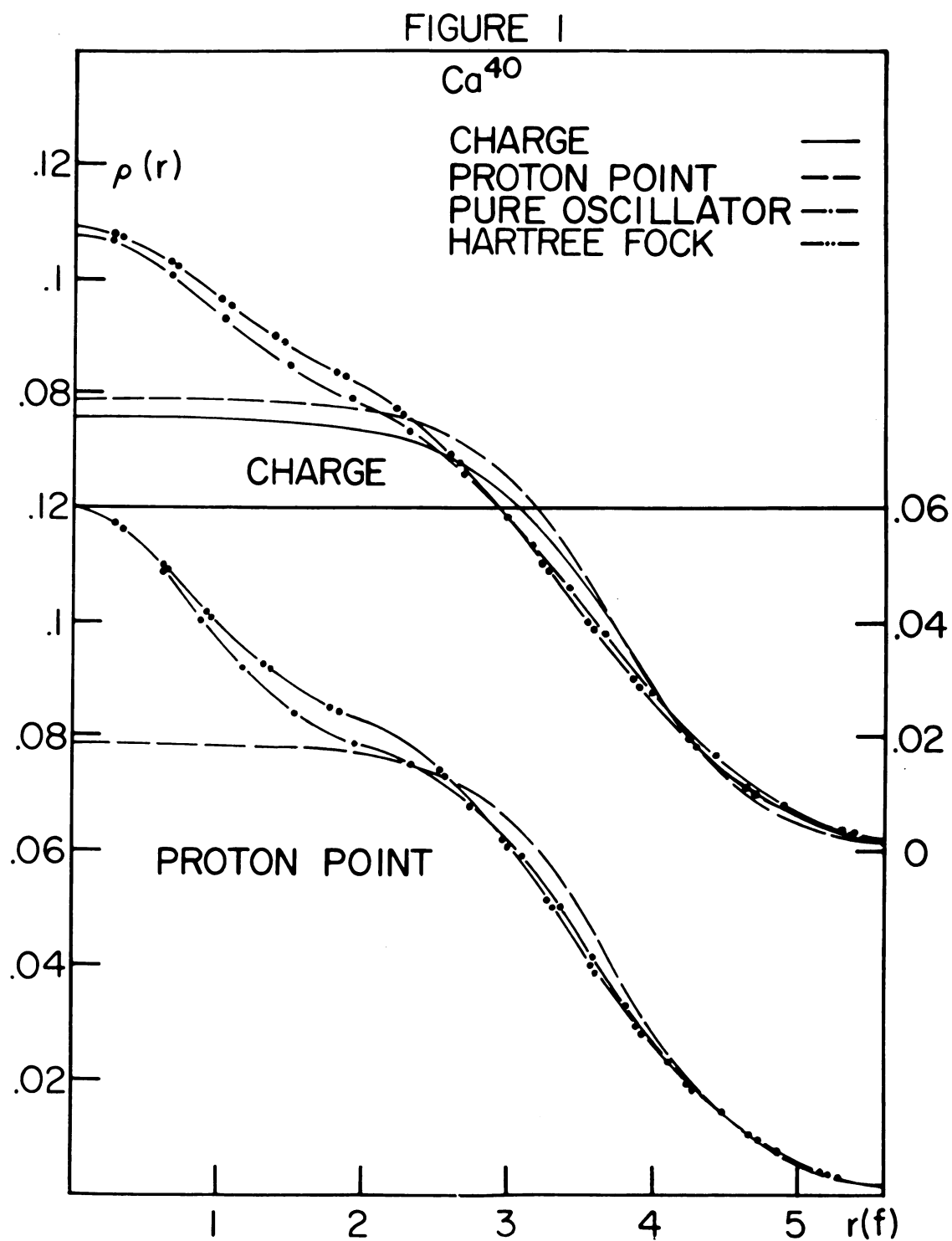
# FIGURE I



Figure 1. The charge and proton point distribution for ⁴⁰Ca compared to the distributions obtained by pure oscillator functions and Hartree-Fock functions.

# FIGURE 2
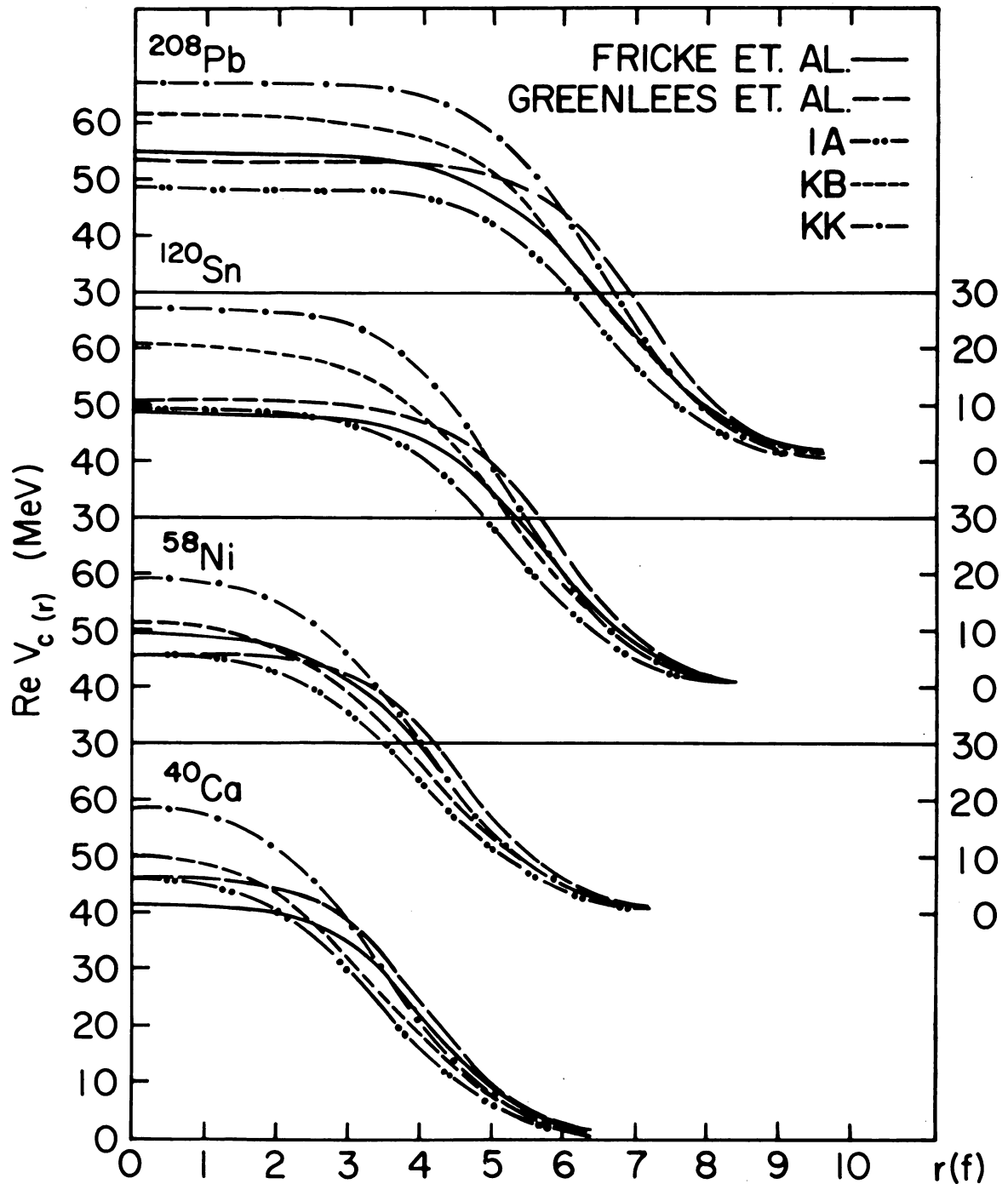


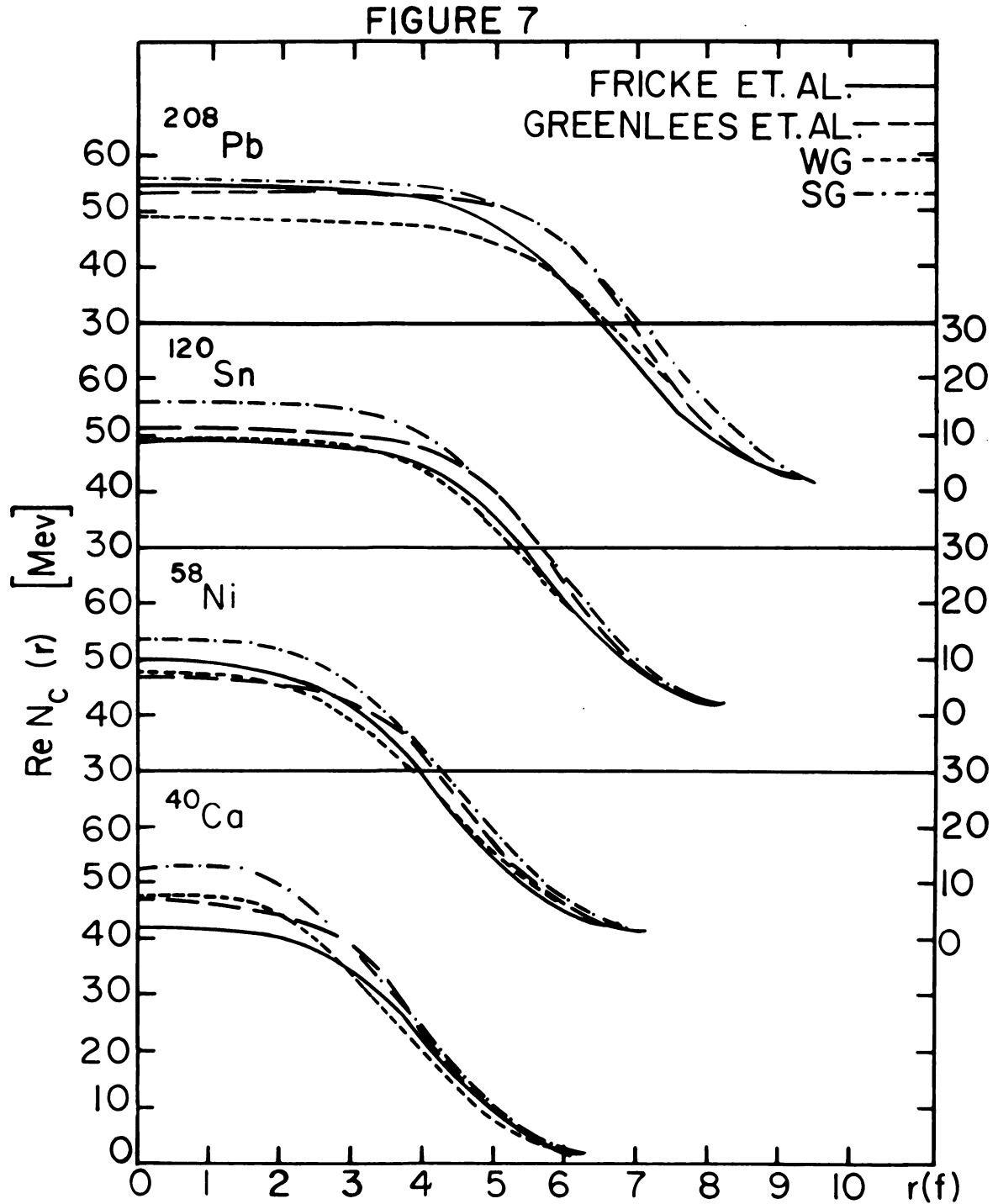Figure 2. The theoretical real central potentials of IA, KB, and KK with no antisymmetrization and no density difference are compared to the empirical potentials of Fricke et al and Greenlees et al.

## FIGURE 3



Figure 3. The theoretical real central potentials of WG and SG with no antisymmetrization and no density difference are compared to the empirical potentials of Fricke et al and Greenlees et al.
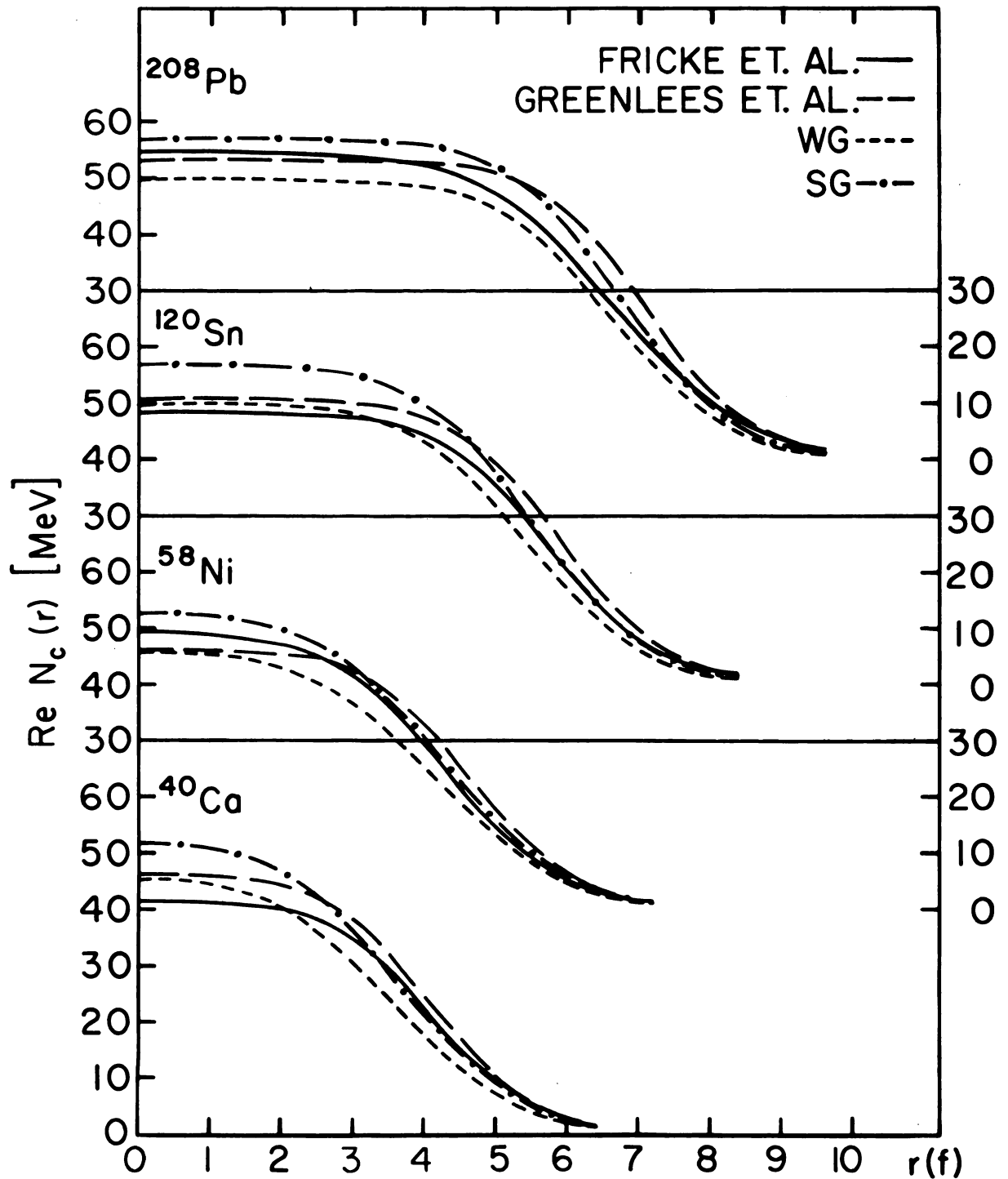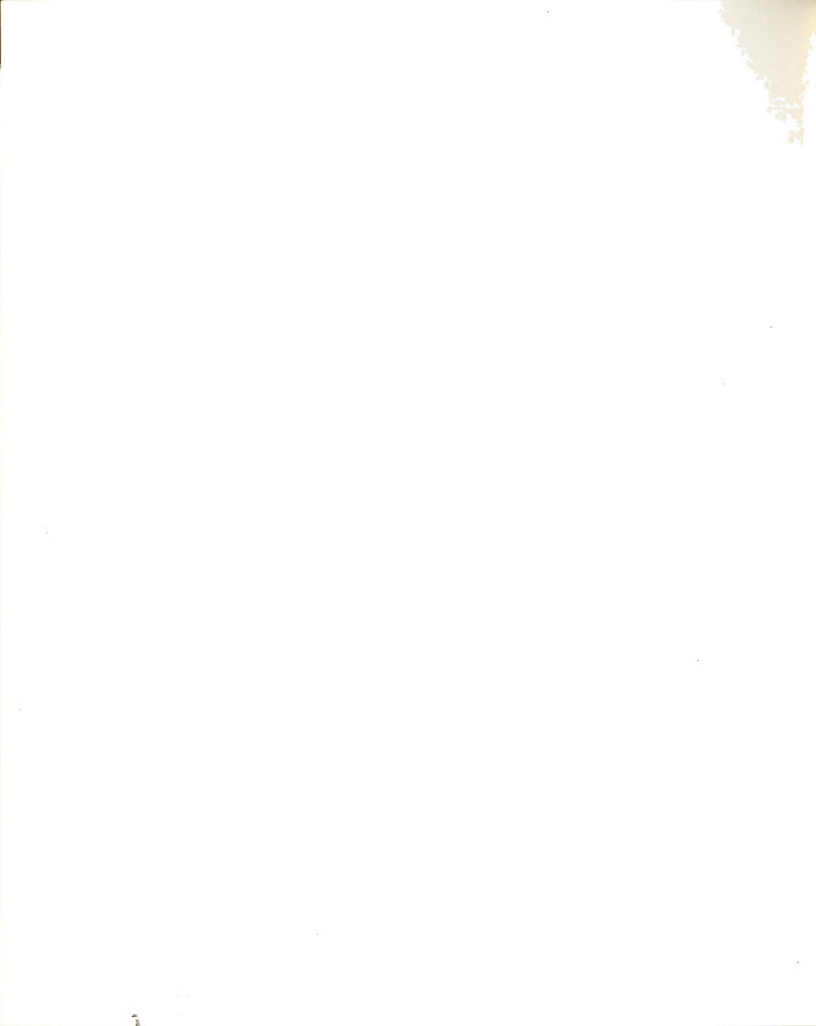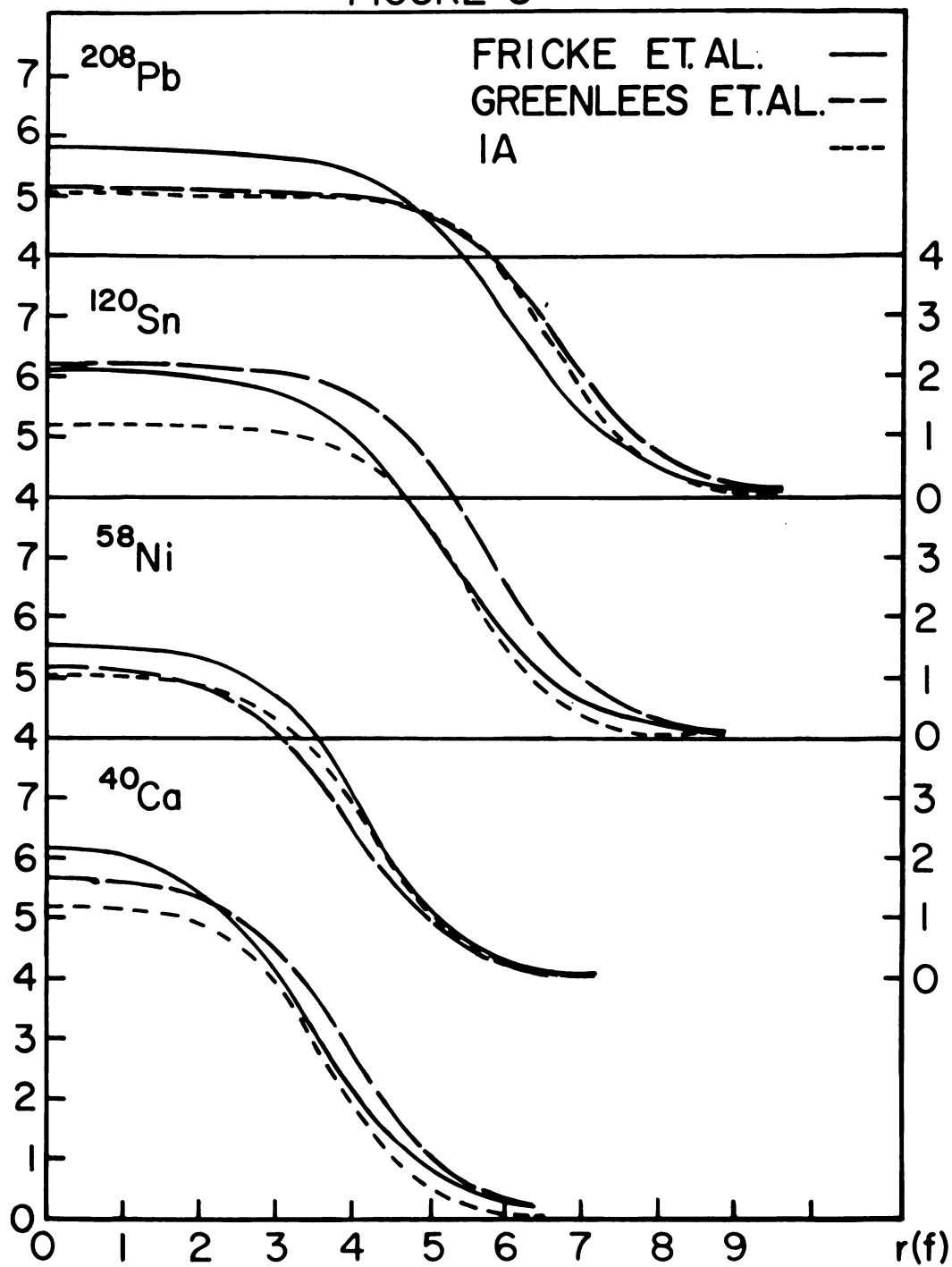
# FIGURE 3



Figure 3. The theoretical real central potentials of WG and SG with no antisymmetrization and no density difference are compared to the empirical potentials of Fricke et al and Greenlees et al.
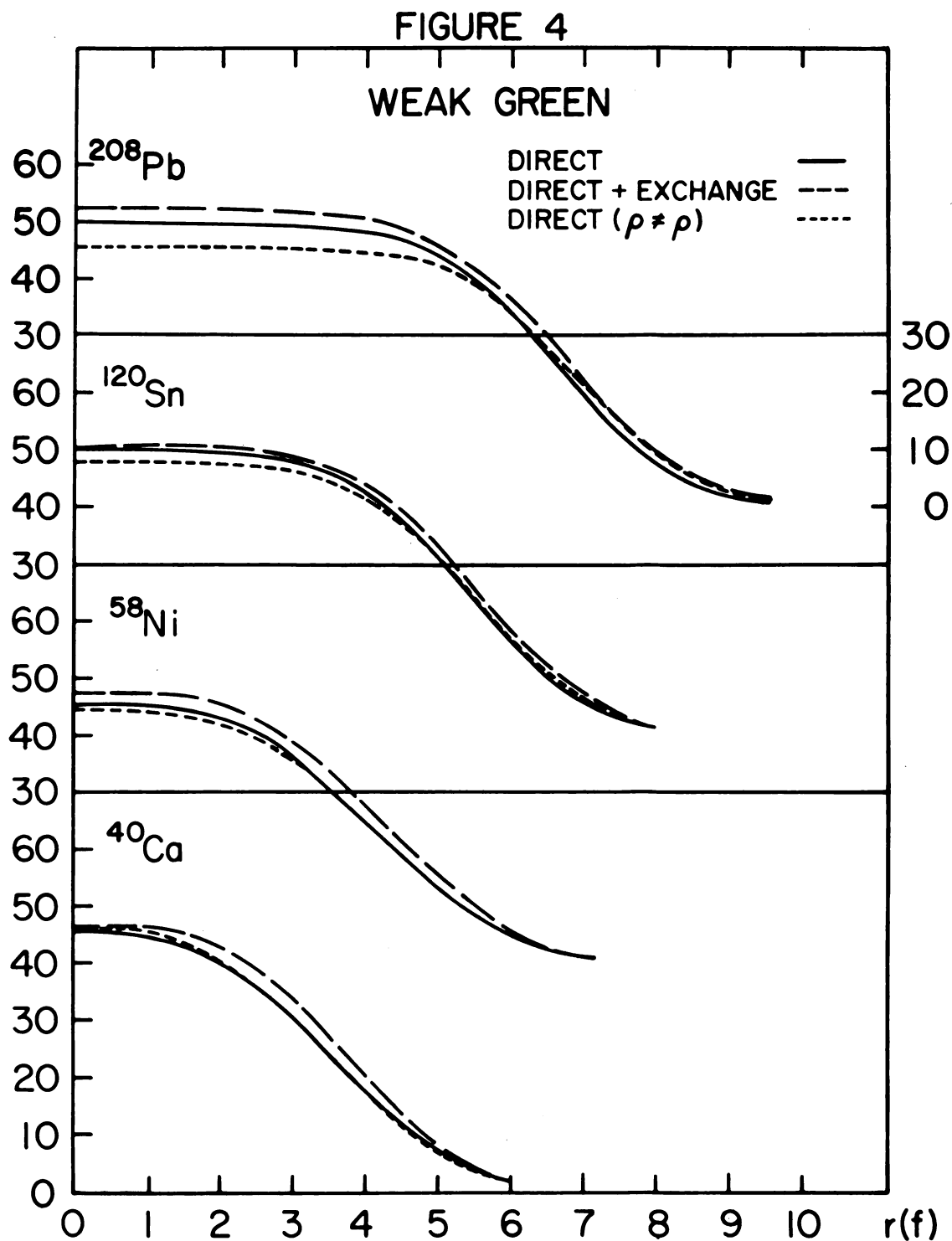
# FIGURE 4



Figure 4. The theoretical real central potential of WG where the effect of antisymmetrization and density difference are included.

65
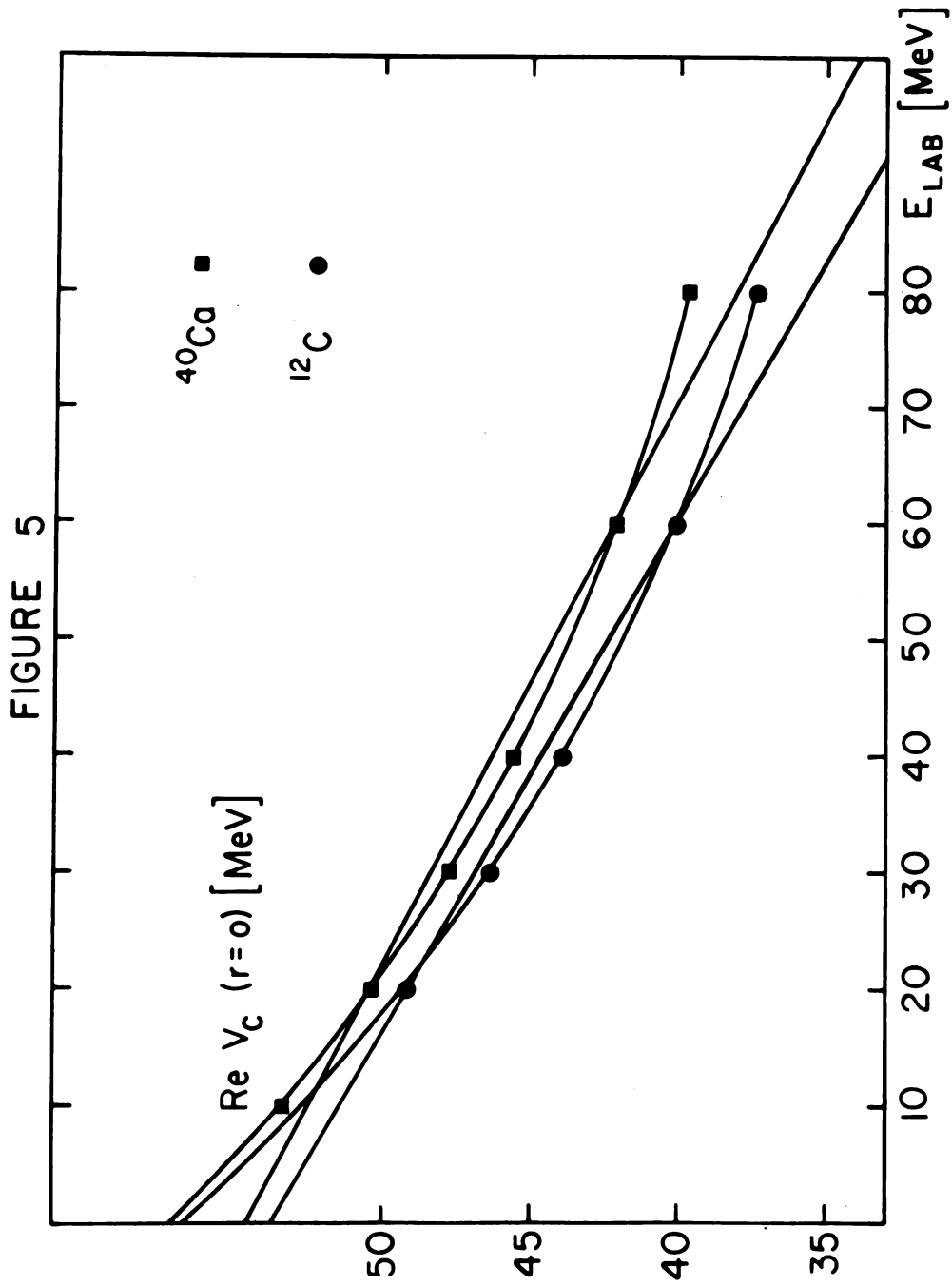


FIGURE 5

Figure 5.  The variation of the strength of the real central potential with energy for $^{12}$C and $^{40}$Ca using the WG effective interaction.

FIGURE 6

WEAK GREEN
$^{40}Ca$

20MeV ——
40MeV – –

Re $V_c(r)$ [MeV]

r(f)
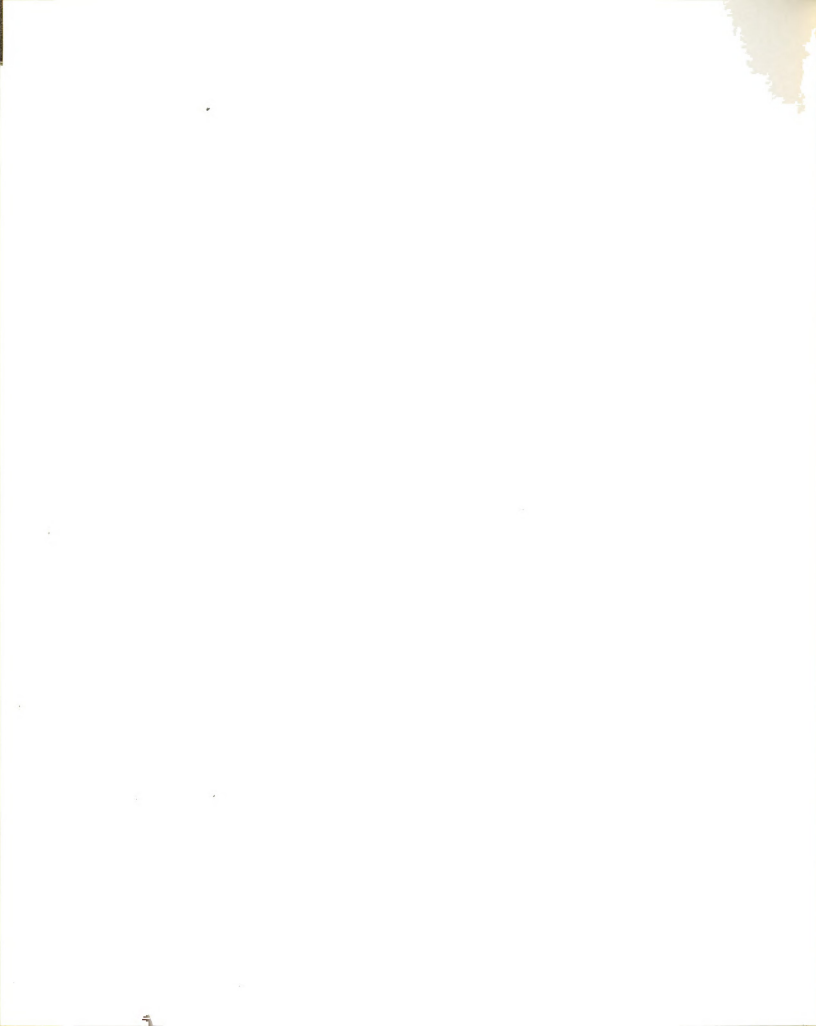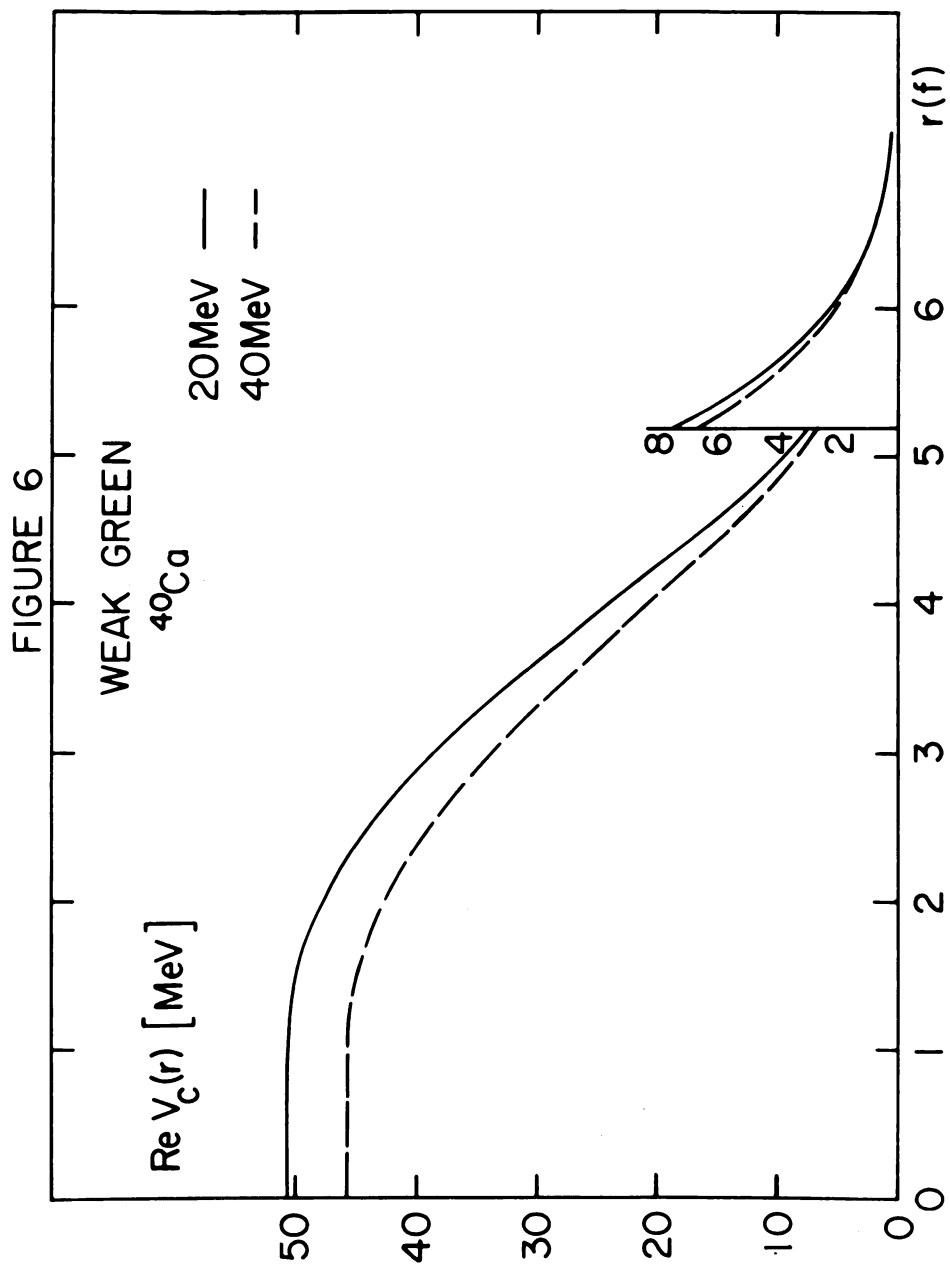
Figure 6. The real central potential of WG for $^{40}Ca$ at the lab energies of 20 and 40 MeV.

# FIGURE 7



Figure 7. The theoretical real central potentials of WG and SG with anitsymmetrization and density difference are compared to the empirical potentials of Fricke et al and Greenlees et al.

# FIGURE 8



Figure 8. The real spin orbit potential of IA is compared to the empirical potentials of Fricke et al and Greenlees et al.
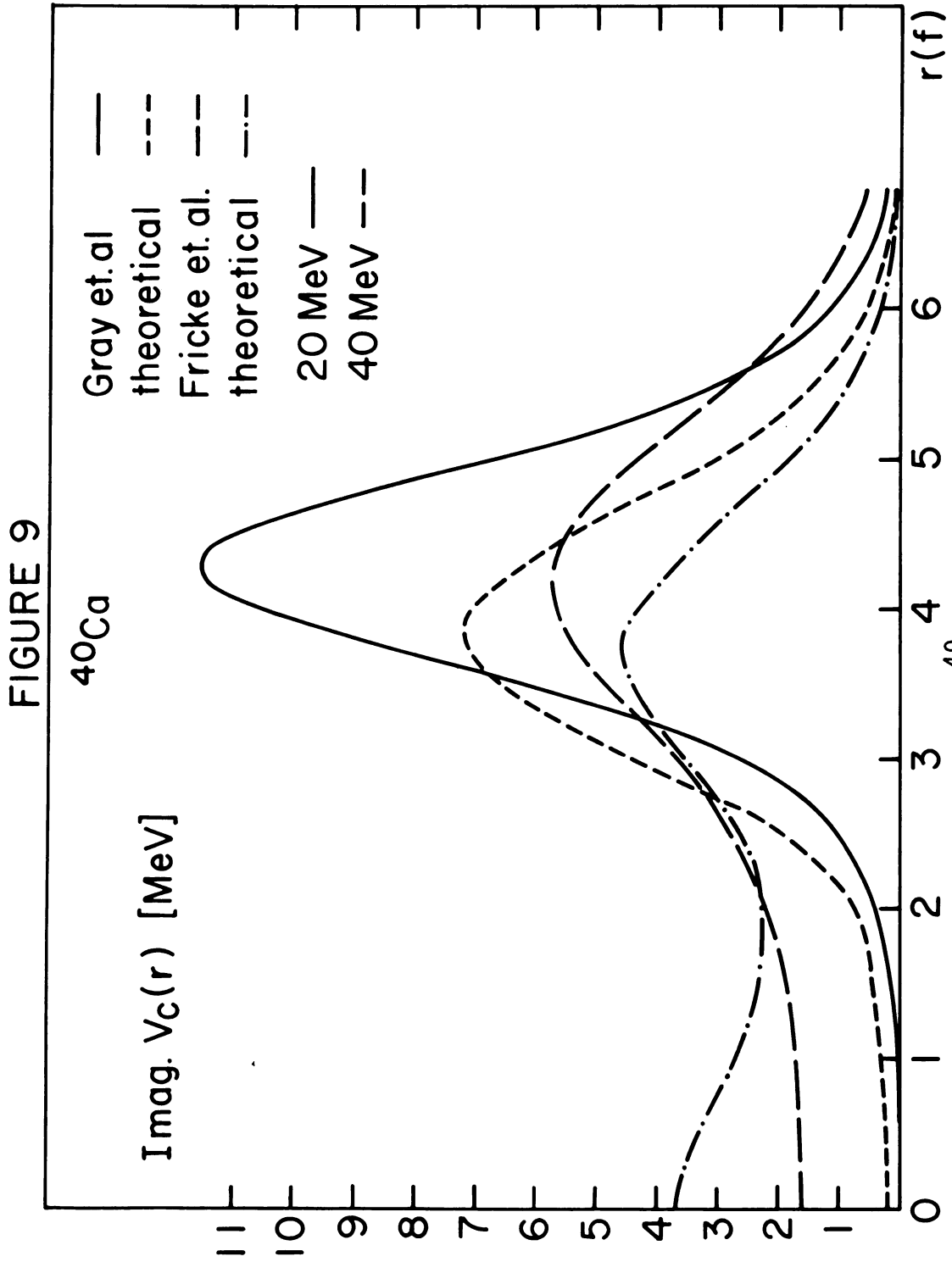
FIGURE 9

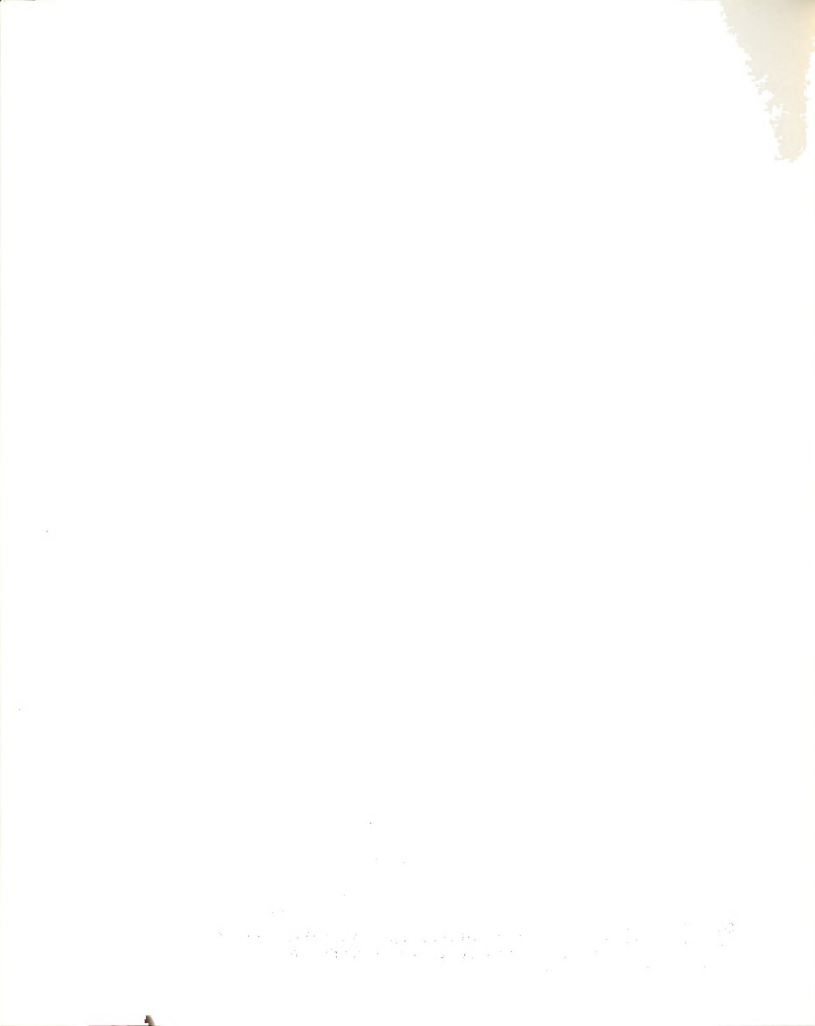Figure 9. The imaginary central for $^{40}$Ca at 20 and 40 MeV are compared to the empirical potentials of Gray et al. and Fricke et al.
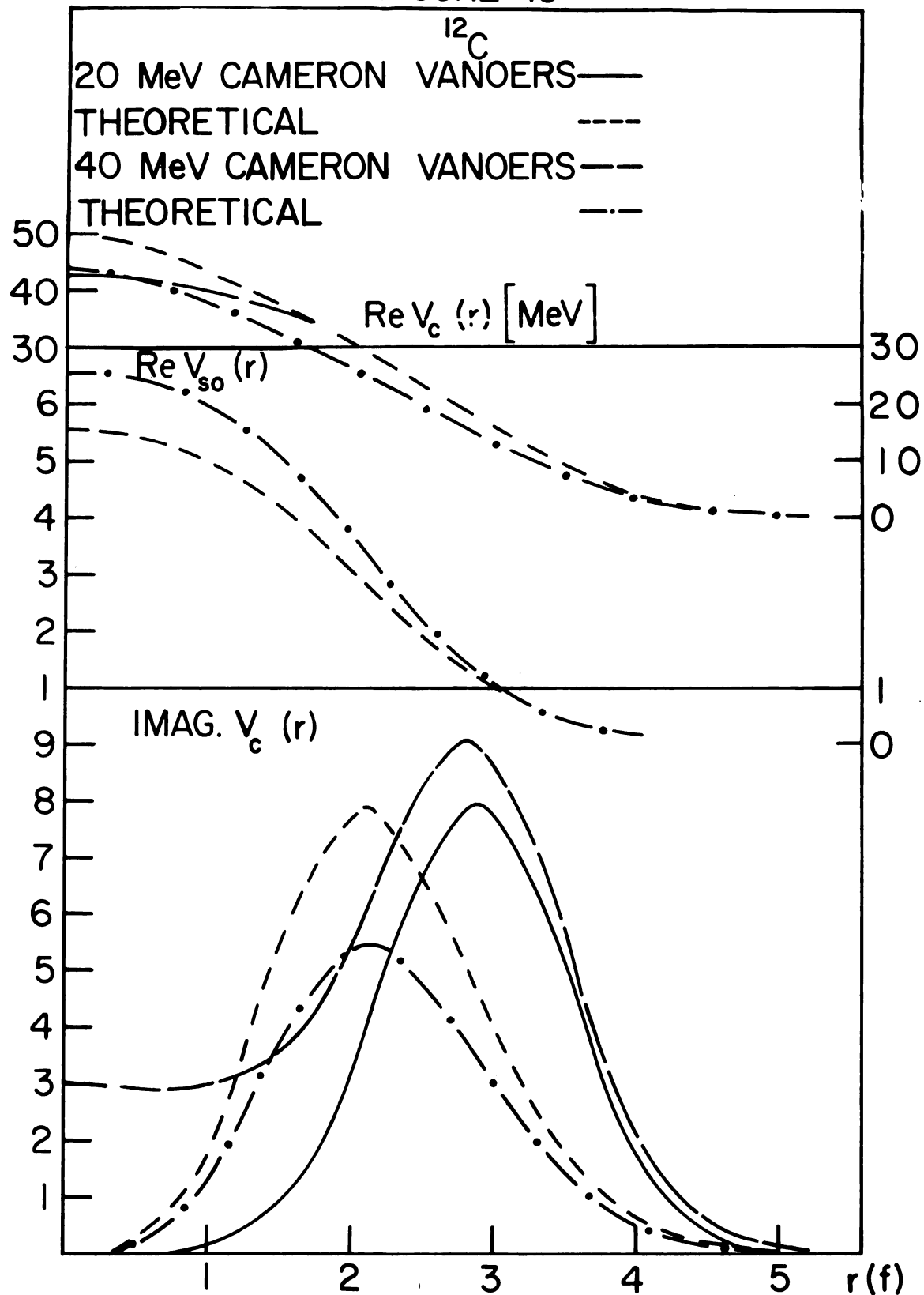
Figure 10. The theoretical optical potentials for $^{12}$C at 20 and 40 MeV are compared to the empirical potentials of Cameron and van Oers.
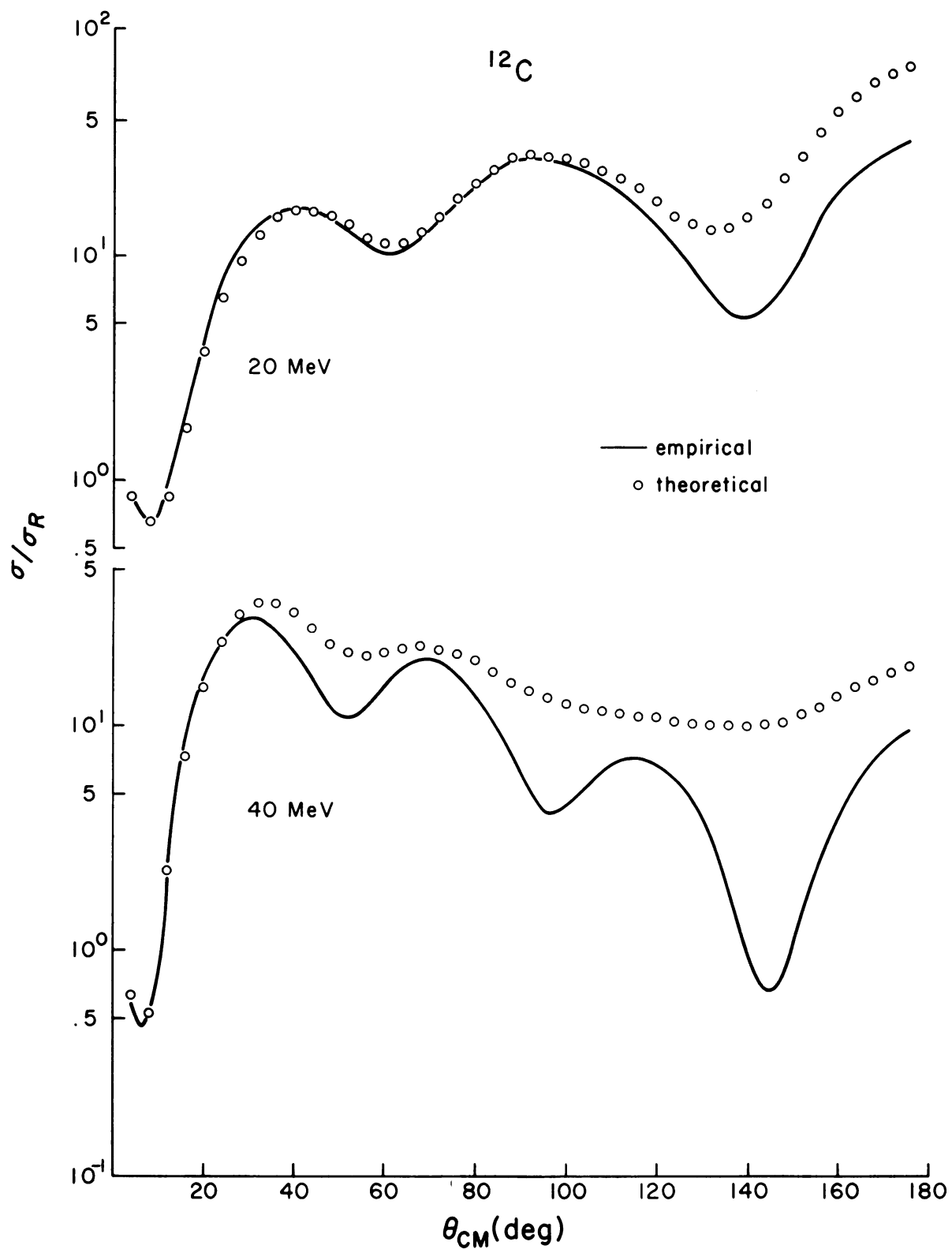
Figure 11.  The cross section for $^{12}$C at 20 and 40 MeV for the theoretical optical potential compared to the potential of Cameron and van Ores.
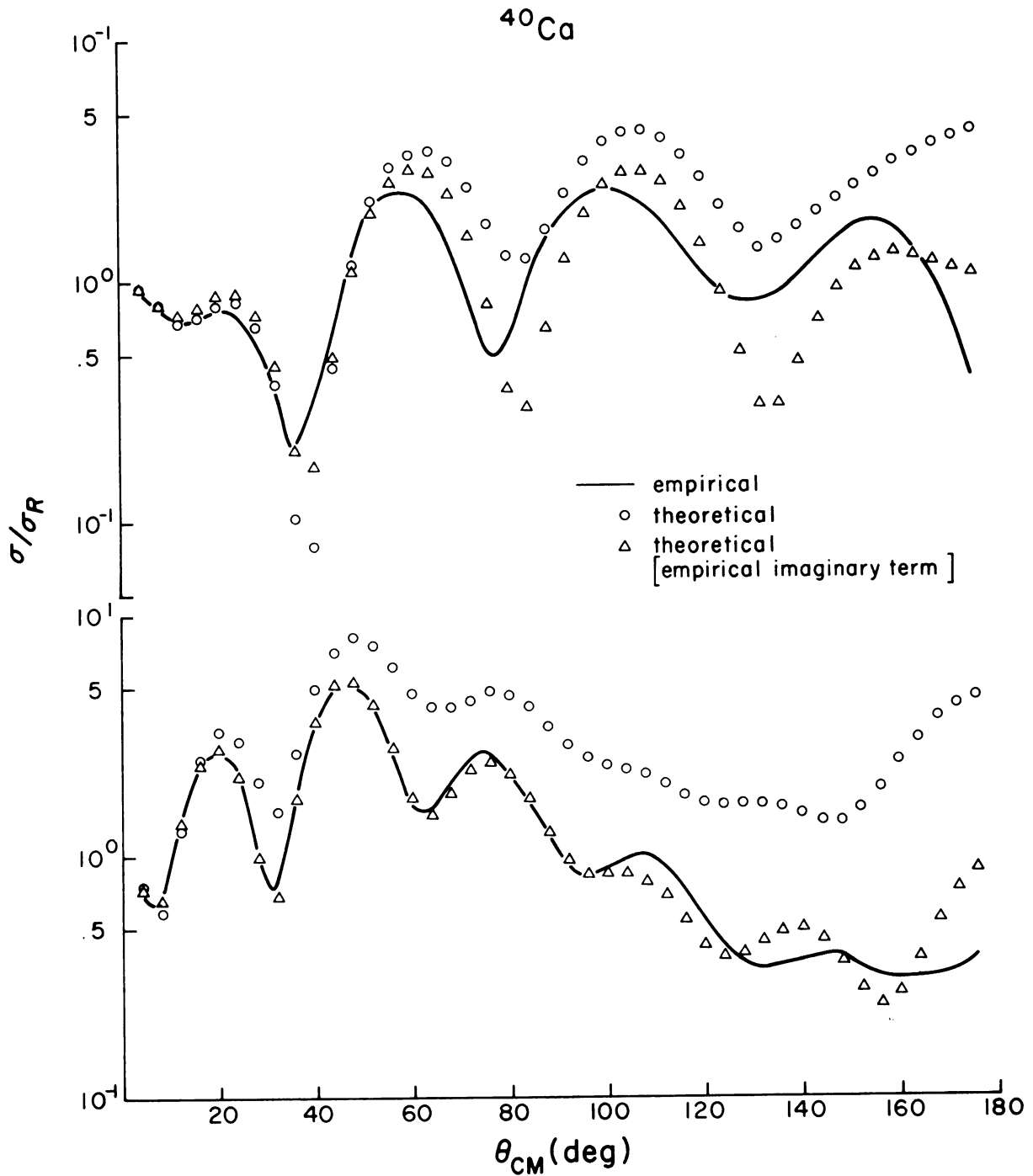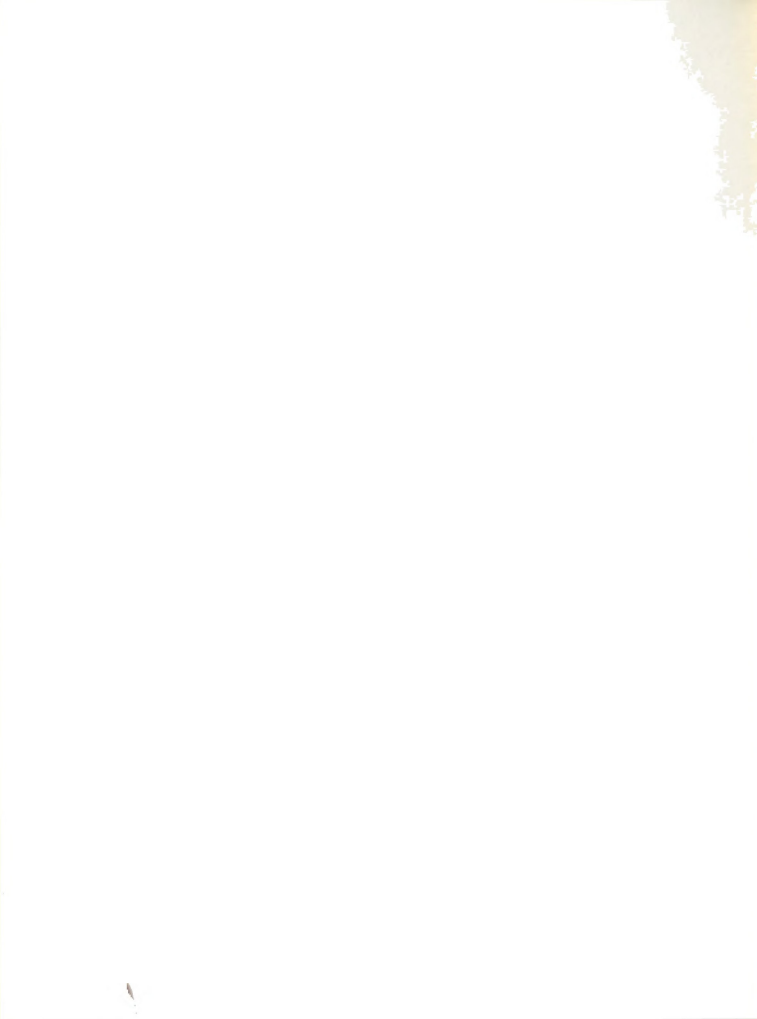
Figure 12. The cross section for $^{40}$Ca at 20 and 40 MeV for the theoretical optical potential compared to the potential of Gray et al and Fricke et al. The crosses denote the theoretical potential with the imaginary term being replaced by its empirical counterpart.